Molecular Therapy
Original Article

AMPK Complex Activation Promotes Sarcolemmal Repair in Dysferlinopathy

Hiroya Ono,[1] Naoki Suzuki,[1] Shin-ichiro Kanno,[2] Genri Kawahara,[3] Rumiko Izumi,[1] Toshiaki Takahashi,[4] Yasuo Kitajima,[5] Shion Osana,[6] Naoko Nakamura,[1] Tetsuya Akiyama,[1] Kensuke Ikeda,[1] Tomomi Shijo,[1] Shio Mitsuzawa,[1] Ryoichi Nagatomi,[6] Nobukazu Araki,[7] Akira Yasui,[2] Hitoshi Warita,[1] Yukiko K. Hayashi,[3] Katsuya Miyake,[7,8] and Masashi Aoki[1]

[1]Department of Neurology, Tohoku University School of Medicine, Sendai 980-8574, Japan; [2]The Institute of Development, Aging and Cancer, Tohoku University, Sendai 980-8575, Japan; [3]Department of Pathophysiology, Tokyo Medical University, Tokyo 160-8402, Japan; [4]National Hospital Organization Sendai-Nishitaga Hospital, Sendai 982-8555, Japan; [5]Department of Muscle Development and Regeneration, Division of Developmental Regulation, Institute of Molecular Embryology and Genetics, Kumamoto University, Kumamoto 860-0811, Japan; [6]Division of Biomedical Engineering for Health and Welfare, Tohoku University Graduate School of Biomedical Engineering, Sendai 980-8575, Japan; [7]Department of Histology and Cell Biology, Faculty of Medicine, Kagawa University, Kagawa, 761-0793, Japan; [8]Center for Basic Medical Research, Narita Campus, International University of Health and Welfare, Narita 286-8686, Japan

Mutations in *dysferlin* are responsible for a group of progressive, recessively inherited muscular dystrophies known as dysferlinopathies. Using recombinant proteins and affinity purification methods combined with liquid chromatography-tandem mass spectrometry (LC-MS/MS), we found that AMP-activated protein kinase (AMPK)γ1 was bound to a region of dysferlin located between the third and fourth C2 domains. Using *ex vivo* laser injury experiments, we demonstrated that the AMPK complex was vital for the sarcolemmal damage repair of skeletal muscle fibers. Injury-induced AMPK complex accumulation was dependent on the presence of Ca^{2+}, and the rate of accumulation was regulated by dysferlin. Furthermore, it was found that the phosphorylation of AMPKα was essential for plasma membrane repair, and treatment with an AMPK activator rescued the membrane-repair impairment observed in immortalized human myotubes with reduced expression of dysferlin and dysferlin-null mouse fibers. Finally, it was determined that treatment with the AMPK activator metformin improved the muscle phenotype in zebrafish and mouse models of dysferlin deficiency. These findings indicate that the AMPK complex is essential for plasma membrane repair and is a potential therapeutic target for dysferlinopathy.

INTRODUCTION

Dysferlinopathies are a group of progressive, recessively inherited muscular dystrophies that include Miyoshi myopathy,[1,2] limb-girdle muscular dystrophy (LGMD) type 2B,[3,4] and distal anterior compartment myopathy.[5] These conditions are caused by mutations in the gene encoding *dysferlin*, a transmembrane protein consisting of seven C2 domains, three Fer domains, and two DysF domains.[6] In humans, dysferlin is highly expressed in the skeletal and cardiac muscles.[3] The impaired healing of membrane disruption in the muscle fibers of dysferlin-deficient mice indicates that dysferlin is involved in plasma membrane repair.[7–9]

The pathogenic *dysferlin* mutations reported in patients to date have been shown to decrease the protein levels of dysferlin in skeletal muscles.[6] A marked reduction in the levels of dysferlin due to missense mutations suggests that the mutated protein is recognized and degraded by the quality control system in the cell.[10] Additionally, the expression of full-length dysferlin has been reported to rescue these cells from the pathological characteristics of dysferlinopathy *in vitro*.[11] These studies highlight the importance of investigating loss-of-function mechanisms in the exploration of therapeutic strategies for dysferlinopathy.

To date, numerous candidate dysferlin-binding proteins, such as AHNAK,[12,13] caveolin 3,[14] vinculin,[15] mitsugumin 53 (MG53; also known as TRIM72),[16] and annexins,[17] have been identified. It appears that these are involved in various aspects of the dysferlin-mediated repair pathway, including intracellular vesicle aggregation and trafficking, in addition to the targeting and fusion of a hydrophobic patch to the breached plasma membrane.

We hypothesized that membrane-bound dysferlin serves as a scaffold protein for functional molecules and that the dysferlin-binding partner is pivotal in plasma membrane repair. The present study aimed to identify a binding partner for dysferlin, and thus provide novel insights into the underlying mechanism of defected plasma membrane repair in dysferlinopathy.

Received 13 September 2019; accepted 6 February 2020;
https://doi.org/10.1016/j.ymthe.2020.02.006.

Correspondence: Masashi Aoki, MD, PhD, Department of Neurology, Tohoku University School of Medicine, 1-1 Seiryo-machi, Sendai 980-8574, Japan.
E-mail: aokim@med.tohoku.ac.jp
Correspondence: Shin-ichiro Kanno, PhD, The Institute of Development, Aging and Cancer, Tohoku University, 4-1 Seiryo-machi, Sendai 980-8575, Japan.
E-mail: shinichiro.kanno.a6@tohoku.ac.jp

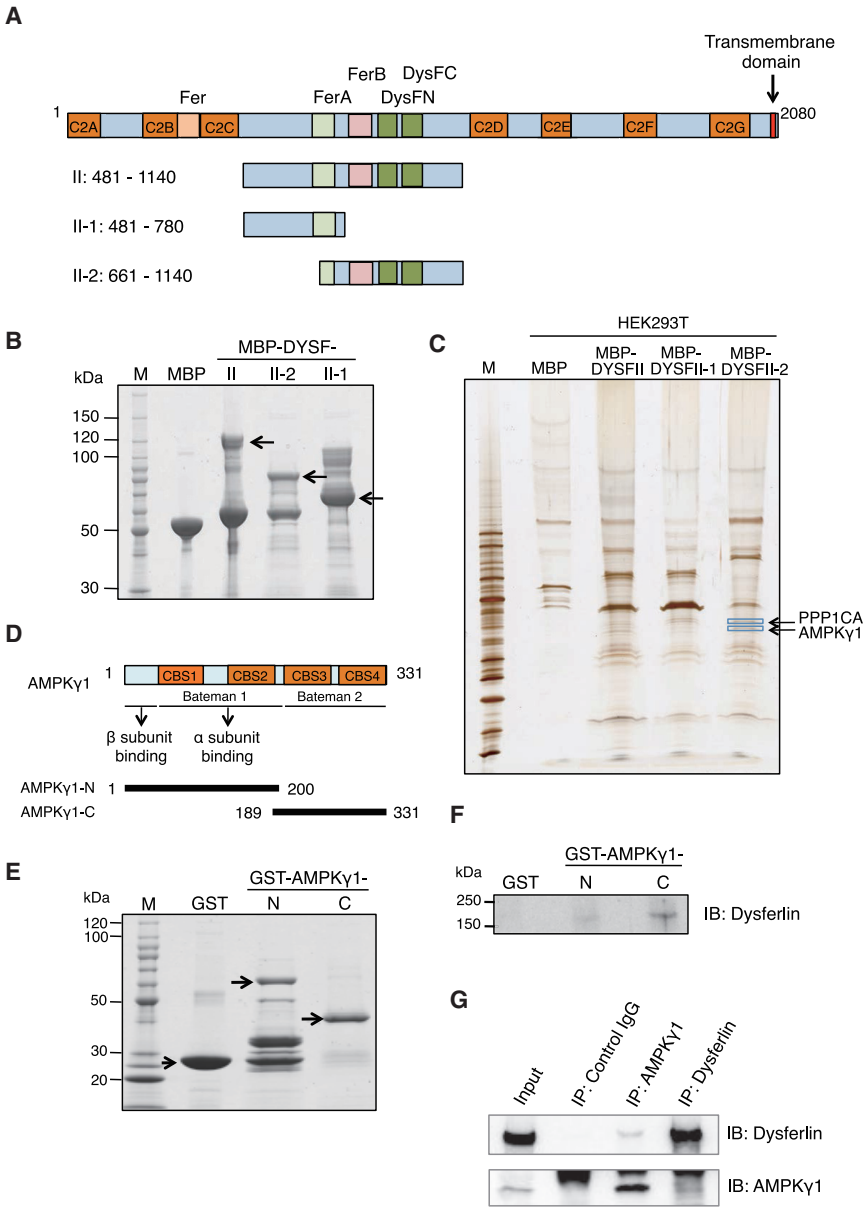

Figure 1. AMPKγ1 Interacts with Dysferlin *In Vitro*

(A) Schema of the human dysferlin domain structures. Seven C2 domains, three Fer domains, and two DysF domains are present. The transmembrane (TM) region is located at the C terminus. The region between C2C and C2D is designated as the II region. In subsequent experiments, the II region was divided into two parts (II-1 and II-2). (B) Coomassie blue-stained blot of generation of MBP fusion proteins for the II region of dysferlin. Arrows indicate bands of interests. M, molecular weight marker; MBP, MBP control. (C) HEK293T cell lines were affinity purified using MBP columns. Co-precipitated proteins were separated by SDS-PAGE and silver stained. Using LC-MS/MS, several bands, including PPP1CA and AMPKγ1, were found to bind to the II region. (D) Schema of the human AMPKγ1 domain structure. Four cystathionine beta-synthase (CBS) domains are present.[18] AMPKγ1 was divided into two parts (AMPKγ1-N and AMPKγ1-C) for subsequent experiments. CBS domains were always found in pairs within protein sequences, and each pair was tightly associated through its β sheets in a pseudo-dimeric arrangement, forming a Bateman domain.[19] (E) Coomassie blue-stained blot of generation of GST-fused recombinant proteins for AMPKγ1-N and AMPKγ1-C. Arrows indicate bands of interest. (F) Mouse skeletal muscle homogenates were affinity purified using GST columns. Co-precipitated proteins were separated by SDS-PAGE. Dysferlin was detected in the GST-AMPKγ1-C column and weakly detected in the GST-AMPKγ1-N column. (G) AMPKγ1 interacts endogenously with dysferlin. Cell lysates of the mouse skeletal muscle were immunoprecipitated with anti-AMPKγ1 antibody, anti-dysferlin antibody, or control IgG and analyzed via immunoblotting with anti-dysferlin and anti-AMPKγ1 antibodies.

RESULTS

Identification of AMPKγ1 as a Dysferlin-Binding Protein

Human dysferlin is a large membrane protein with a molecular mass of 230 kDa comprising seven C2 domains that bind to the lipid bilayer of the sarcolemma (Figure 1A). Considering that the II region consists of 660 aa (amino acids 481–1140), the region was divided into two parts for experiments in the present study (Figure 1A). These regions were then subcloned into plasmids (primers are listed in Table S1). Maltose-binding protein (MBP)-tagged recombinant proteins containing the II region were expressed in *Escherichia coli* (arrows in Figure 1B). The lysates from HEK293T cells were then mixed with the tagged proteins and immunoprecipitated with anti-MBP magnetic beads. The co-precipitated proteins were then separated by SDS-PAGE, silver stained (Figure 1C), and analyzed using liquid chromatography-tandem mass spectrometry (LC-MS/MS). Of the 10 proteins analyzed, AMP-activated protein kinase (AMPK)γ1 and protein phosphatase (PPP) 1CA were identified in dysferlin co-precipitates (Figure 1C). The observed co-precipitation of AMPKγ1 and PPP1CA with dysferlin suggested that the AMPK complex might be involved in the function of dysferlin and membrane repair.

To examine whether AMPKγ1 specifically binds to dysferlin in skeletal muscles, the products of the co-precipitation assays were subjected to anti-dysferlin immunoblotting. Glutathione *S*-transferase (GST)-tagged recombinant proteins containing the N- or C-terminal region of AMPKγ1 were expressed in *E. coli* (Figures 1D and 1E). Lysates of mouse skeletal muscle were mixed with the tagged proteins and immunoprecipitated with anti-GST magnetic beads. The co-precipitated proteins were then separated by SDS-PAGE. Dysferlin was detected in the chromatographic fraction of the AMPKγ1 C-terminal region and weakly detected in

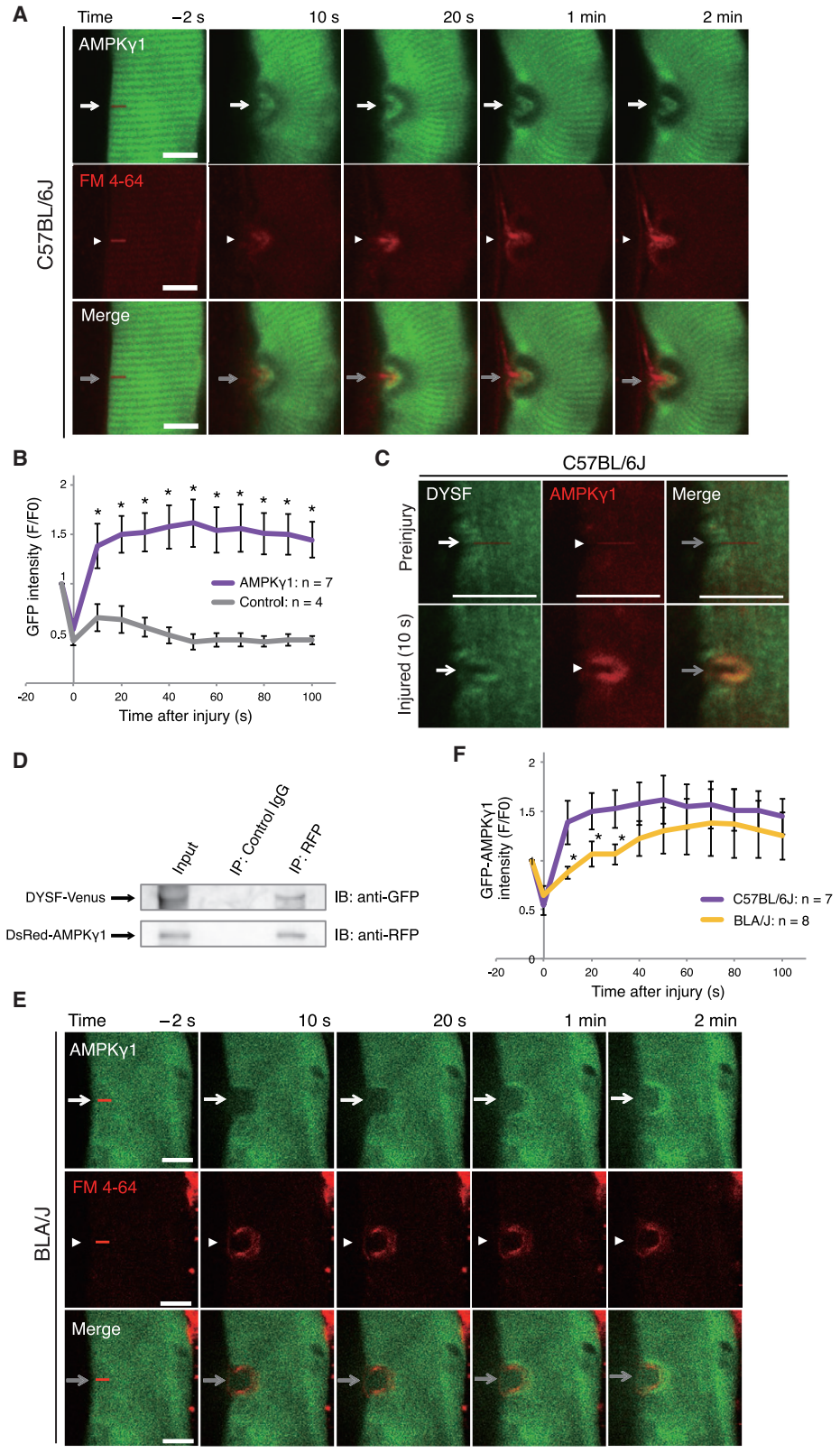

(legend on next page)

the N-terminal region using a monoclonal anti-dysferlin antibody (Figure 1F).

To examine whether AMPK is associated with endogenously expressed dysferlin, the cell lysates of the mouse skeletal muscle were immunoprecipitated with an anti-AMPKγ1 antibody, anti-dysferlin antibody, or control immunoglobulin G (IgG), and the precipitates were then analyzed by immunoblotting with anti-dysferlin and anti-AMPKγ1 antibodies. Endogenous dysferlin was detected with the anti-dysferlin antibody, and endogenous AMPKγ1 was detected with the anti-AMPKγ1 antibody in the immunoprecipitates, but not in those with control IgG (Figure 1G; full blot in Figure S1). These results indicate the association between dysferlin and AMPKγ1 in mouse skeletal muscle tissue.

Dysferlin Regulates the Rate of Recruitment of AMPKγ1 to the Injured Plasma Membrane Site

We investigated whether the AMPK complex is involved in membrane repair, given that its binding partner, dysferlin, serves a key role in sarcolemmal repair.[8] To directly evaluate the dynamic process of membrane repair in living myofibers, the plasma membrane of myofibers transduced with GFP-tagged AMPKγ1 was mechanically injured using a two-photon laser in the presence of the FM4-64 fluorescent dye. The site of injury (red line at −2 s in Figure 2A) was identified as the site of FM4-64 accumulation (white arrowheads in Figure 2A). Rapid (<10 s) and localized recruitment of GFP-AMPKγ1 to the site of injury was observed (white arrows in Figure 2A), with GFP-AMPKγ1 surrounding the injury site (merged images in Figure 2A; Video S1). However, no localized recruitment of unconjugated GFP (control) was observed (Figure S2A). Quantification of the GFP-AMPKγ1 signal at the site of FM4-64 accumulation revealed that the fluorescence intensity of GFP-AMPKγ1 was significantly higher than that of unconjugated GFP (Figure 2B).

A previous study reported that dysferlin-GFP is recruited to myofibers within 5 s of injury.[20] As AMPKγ1 and dysferlin share a similar pattern of rapid accumulation at injury sites, we investigated whether dysferlin has an active role in the accumulation of AMPKγ1. To examine the biological function of the association between dysferlin and AMPKγ1 in sarcolemmal repair, membrane-repair assays were performed using mouse skeletal muscle co-transfected with Venus-tagged dysferlin and DsRed-tagged AMPKγ1. Dysferlin was recruited to the membrane region within 5 s following injury, and the accumulation of AMPKγ1 was partially co-localized with dysferlin at the membrane region (Figure 2C; Figures S3 and S4). The results of the co-immunoprecipitation assays indicated that dysferlin and AMPKγ1 form a protein complex when co-expressed in mouse skeletal muscle (Figure 2D). To determine whether dysferlin regulates the injury-induced accumulation of AMPKγ1, this accumulation was examined in the absence of dysferlin. Membrane-repair assays involving the use of GFP-AMPKγ1 in the presence of FM4-64 fluorescent dye revealed that GFP-AMPKγ1 accumulated more slowly (>30 s) in the injured myofibers of dysferlin-deficient BLA/J mice[21] than in C57BL/6J control mice (Figure 2E; Video S2). Quantification of the GFP-AMPKγ1 signal at the site of injury, which was also the site of FM4-64 accumulation, revealed a significant decrease in the fluorescence intensity of BLA/J myofibers until 30 s after injury (Figure 2F), which indicates that the rate of accumulation of AMPKγ1 is regulated by dysferlin.

AMPK Complex Is Recruited to the Injury Site

The role of the AMPK catalytic α subunit in membrane repair was examined. Using experiments similar to those conducted on regulatory subunit AMPKγ1, we investigated the catalytic subunits AMPKα1 and AMPKα2, which were frequently observed to accumulate at the injury site of damaged myofibers (Figures S5A, S6, and S7A). Rapid (<10 s) and localized recruitment of GFP-AMPKα1 to the site of injury was observed (white arrows in Figure S5A), with GFP-AMPKα1 surrounding the injury site, similar to AMPKγ1 (merged images in Figure S5A; Video S3). Quantification of the GFP-AMPKα1 signal at the site of injury, identified as the site of FM4-64 accumulation, revealed that the fluorescence intensity of GFP-AMPKα1 was significantly higher than that of unconjugated GFP (control) (Figure S5B).

The morphology of accumulated GFP-AMPKα1 is affected by slight differences in parameters, such as laser strength, laser angle, and cell thickness. The forms of the accumulation were mainly a C-shape, circle, and line (Figure S6). It was observed that plasma membrane wounding was occasionally followed by rapid formation of a localized bleb in the muscle fiber of wild-type (WT) mice. A previous study reported that the occurrence of membrane blebbing in response to hypotonic shock required the presence of dysferlin in human- and mouse-cultured myotubes.[22] Another group reported that membrane

Figure 2. AMPKγ1 Is Recruited to the Injured Plasma Membrane and Its Rate Is Regulated by Dysferlin

(A) Isolated FDB myofibers from C57BL/6J mice expressing the fluorescently tagged GFP-AMPKγ1 protein were injured (injury site, red line/arrow at −2 s) using a pulsed laser in the presence of the FM4-64 fluorescent dye. The white arrows indicate the location of the damaged membrane. The injury site is indicated by FM4-64 accumulation (white arrowheads). Scale bars, 10 μm. (B) Quantification of the GFP-AMPKγ1 signal at the membrane injury, shown by the site of FM4-64 accumulation. The fluorescence intensity of GFP-AMPKγ1 was significantly higher than that of the unconjugated GFP (control). GFP-AMPKγ1, n = 7 myofibers (four C57BL/6J mice); control (unconjugated GFP), n = 4 myofibers (two C57BL/6J mice). (C) Dysferlin-Venus (DYSF-Venus) was simultaneously expressed with DsRed-tagged AMPKγ1 in mouse skeletal muscle (FDB of C57BL/6J mice). Isolated FDB myofibers from C57BL/6J were injured (injury site, red line) using a pulsed laser. Scale bars, 10 μm. (D) FDBs of C57BL/6J were co-expressed with DYSF-Venus and DsRed-AMPKγ1. The lysates were immunoprecipitated with anti-RFP magnetic beads. Co-precipitated proteins were detected using anti-GFP or anti-RFP antibodies. (E) Isolated FDB muscle fibers from BLA/J mice expressing fluorescently tagged GFP-AMPKγ1 protein were injured using a pulsed laser. Scale bars, 10 μm. (F) Quantification of the GFP-AMPKγ1 signal at the injury site, indicated by FM4-64 accumulation, revealed a slower increase in the fluorescence intensity in the BLA/J myofibers than that in the C57BL/6J myofibers. The data of fluorescence intensity of the GFP-AMPKγ1 in the C57BL/6J myofibers in (B) was reused. C57BL/6J, seven myofibers (four mice); BLA/J, eight myofibers (four mice). Statistically significant differences (*$p < 0.05$) were determined using the Wilcoxon test. Data are expressed as mean ± SE.

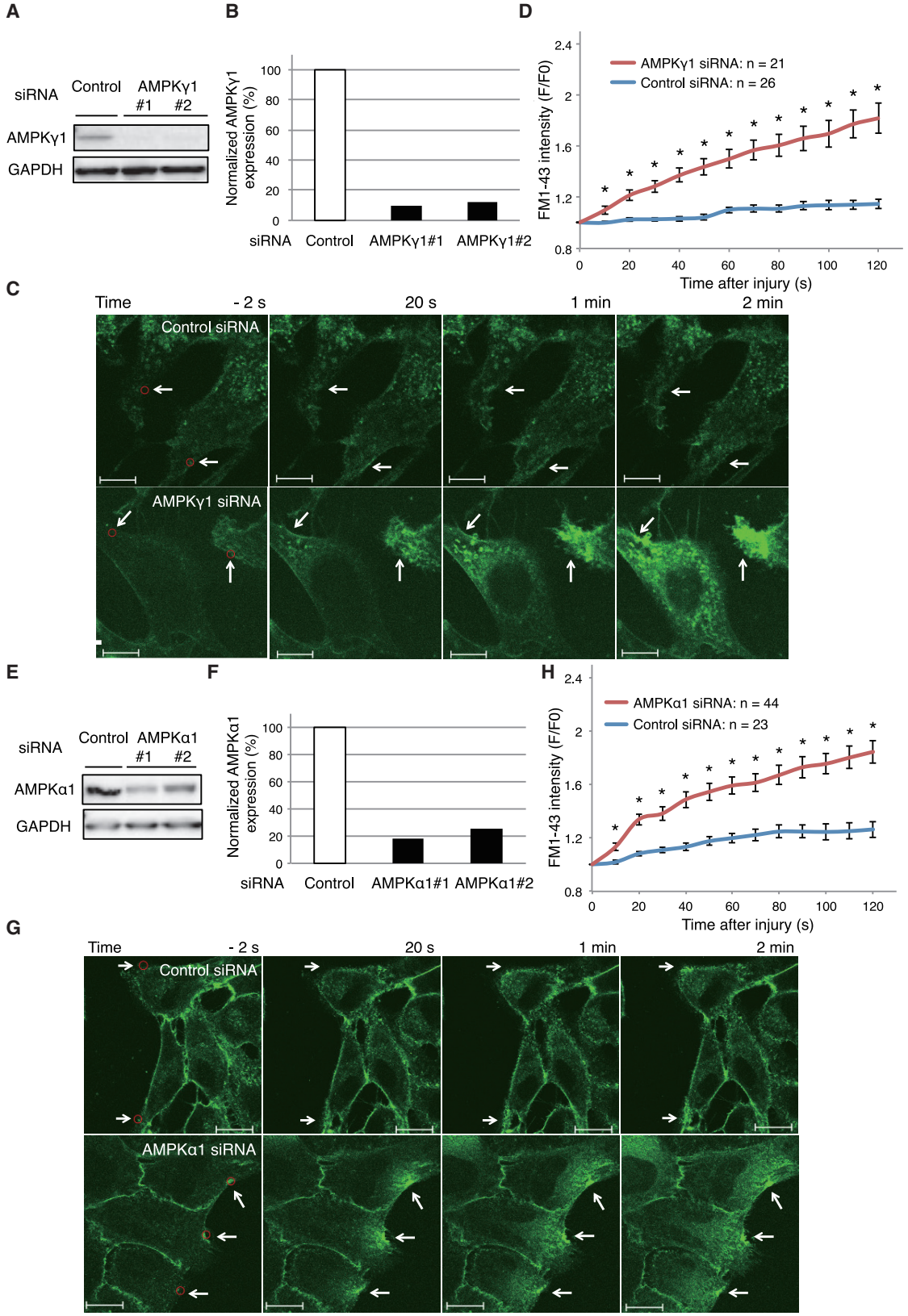

(legend on next page)

blebbing occurred in response to laser injury in HeLa cells.[23] In the present study, the bleb rapidly became positive for DsRed-AMPKγ1 (Figure S4) and negative for unconjugated GFP (control) (Figure S2B). These findings indicate that the AMPK complex accumulates at the site of laser injury.

AMPKγ1 and AMPKα1 Are Required for Effective Membrane Repair in C2C12 Cells

A previous study of laser-induced damage demonstrated a role of dysferlin in the sarcolemmal repair of C2C12 cells.[24] To evaluate the role of AMPKγ1 in the membrane-repair process, the ability of the muscle to recover following laser-induced damage was measured by analyzing the entry of the FM1-43 fluorescent dye into AMPKγ1-knockdown C2C12 cells (Figures 3A–3D; for small interfering RNA [siRNA] targets, refer to Table S2). Using immunoblotting, the knockdown of AMPKγ1 was confirmed (Figures 3A and 3B). WT cells effectively repaired plasma membrane damage (damaged sites are indicated by white arrows in Figure 3C), as the entry of FM1-43 fluorescent dye observed following laser damage was minimal (upper panels in Figure 3C). In contrast, there was significant FM1-43 fluorescent dye entry into the AMPKγ1-knockdown C2C12 cells following laser-induced damage (lower panels in Figure 3C), revealing a defective membrane-repair function. The quantification of FM1-43 revealed significantly increased fluorescence in the AMPKγ1 siRNA-administered C2C12 cells (Figure 3D).

To evaluate the role of the AMPK catalytic α subunit in membrane repair, FM1-43 fluorescent dye was used to assess membrane repair in cells with siRNA-induced knockdown of AMPKα1 and AMPKα2, which was confirmed via immunoblotting (Figures 3E and 3F; Figures S7B and S7C). There was significant FM1-43 fluorescent dye entry into AMPKα1-knockdown C2C12 muscle cells following laser-induced damage (Figures 3G and 3H; Videos S4 and S5), revealing defective membrane repair in these cells. In contrast, FM1-43 intensity was not profoundly affected in AMPKα2-knockdown cells (Figure S7D). These results indicate that both AMPKγ1 and AMPKα1 are important for membrane repair in C2C12 cells.

Injury-Induced Accumulation of AMPKγ1 Is Dependent on Ca^{2+}

Ca^{2+} is essential for wound repair[25] and is likely to be involved in early signaling following membrane damage. As it was established that the cell surface accumulation of dysferlin is triggered by Ca^{2+},[26] the present study examined whether the injury-induced increase in Ca^{2+} also leads to the accumulation of AMPKγ1. Rapid and localized recruitment of GFP-AMPKγ1 to the site of injury was observed in the presence of Ca^{2+} (Figure 2A; Video S1) but not in its absence (Figure 4A; Video S6). Quantification of the GFP-AMPKγ1 signal revealed a lack of fluorescence owing to Ca^{2+} depletion (Figure 4B). Under Ca^{2+}-depleted conditions, no significant difference was observed in the fluorescence intensity between the GFP-AMPKγ1 signal and the unconjugated GFP signal (control) at the site of injury (Figure 4C). These findings indicate that the accumulation of AMPKγ1 is dependent on the presence of Ca^{2+}.

Phosphorylation of AMPKα Is Necessary for Plasma Membrane Repair

To reproduce the membrane wound conditions, we administered ionomycin treatment to mimic Ca^{2+} overflow. The ionomycin-induced Ca^{2+} flux increased the phosphorylation of AMPKα in normal human skeletal muscle myotubes (Figures 5A and 5B). As the administration of compound C (Cc) significantly suppressed the phosphorylation of AMPKα induced by ionomycin treatment (Figures 5A and 5B), Cc was used to examine the effect of the inhibited phosphorylation of AMPKα by Ca^{2+} overflow. Following laser-induced damage, significant FM1-43 fluorescent dye entry into human myotubes was observed following the administration of 10 μM Cc, indicating defective membrane repair (Figure 5C). The quantification of FM1-43 revealed significantly increased fluorescence in the Cc-administered human myotubes (Figure 5D). As with the human myotubes, the administration of Cc significantly suppressed the basal activity of AMPKα phosphorylation in the C57BL/6J myofibers (Figures 5E and 5F). Following laser-induced damage, significant FM1-43 fluorescent dye entry into the mouse skeletal muscle was observed following the administration of 10 μM Cc, indicating defective membrane repair (Figures 5G and 5H). These results led us to test the hypothesis that a phosphorylation of AMPKα is necessary for plasma membrane repair.

AMPK Activators Rescue the Membrane-Repair Defect in Immortalized Myotubes of Patients with Dysferlinopathy and Dysferlin-Deficient Mouse Skeletal Muscle Fibers

The effect of AMPK activators was examined using human immortalized myotubes derived from patients with dysferlinopathy.[27] We used "line 107," which carries compound heterozygous mutations located before the II region that partially expresses dysferlin (Table S3). The

Figure 3. AMPKγ1 and α1 Are Required for Effective Membrane Repair in C2C12 Cells

(A) Western blot analysis of AMPKγ1 expression in C2C12 cells expressing AMPKγ1 or empty siRNA vector. (B) Quantification of AMPKγ1 expression normalized to GAPDH. (C) Following laser injury of myoblasts in the presence of FM1-43 dye, cell membrane repair was monitored by the dye entry. Increased fluorescence was observed in AMPKγ1 knockdown C2C12 cells. The arrows indicate the injury site. Scale bars, 10 μm. (D) Plot showing repair kinetics of the cell membrane (FM1-43 intensity). AMPKγ1 siRNA, n = 21 cells (10 experiments); control siRNA, n = 26 cells (6 experiments). Statistically significant differences (*$p < 0.05$) were determined using the Wilcoxon test. Data are expressed as mean ± SE. (E) Western blot analysis of AMPKα1 expression in C2C12 cells expressing siRNA AMPKα1 or empty siRNA vector. (F) Quantification of AMPKα1 expression normalized to GAPDH. (G) Following laser injury of myoblasts in the presence of an FM dye, cell membrane repair was monitored by following the entry of the dye. Results show an increase in FM1-43 dye fluorescence. Cellular dye fluorescence was normalized to levels before the injury. The arrows indicate the location of the damaged membrane. Scale bars, 10 μm. (H) Plot showing cell membrane-repair kinetics (FM1-43 intensity). AMPKα1 siRNA, n = 44 cells (15 experiments); control siRNA, n = 23 cells (5 experiments). Statistically significant differences (*$p < 0.05$) were determined using the Wilcoxon test. Data are expressed as mean ± SE.

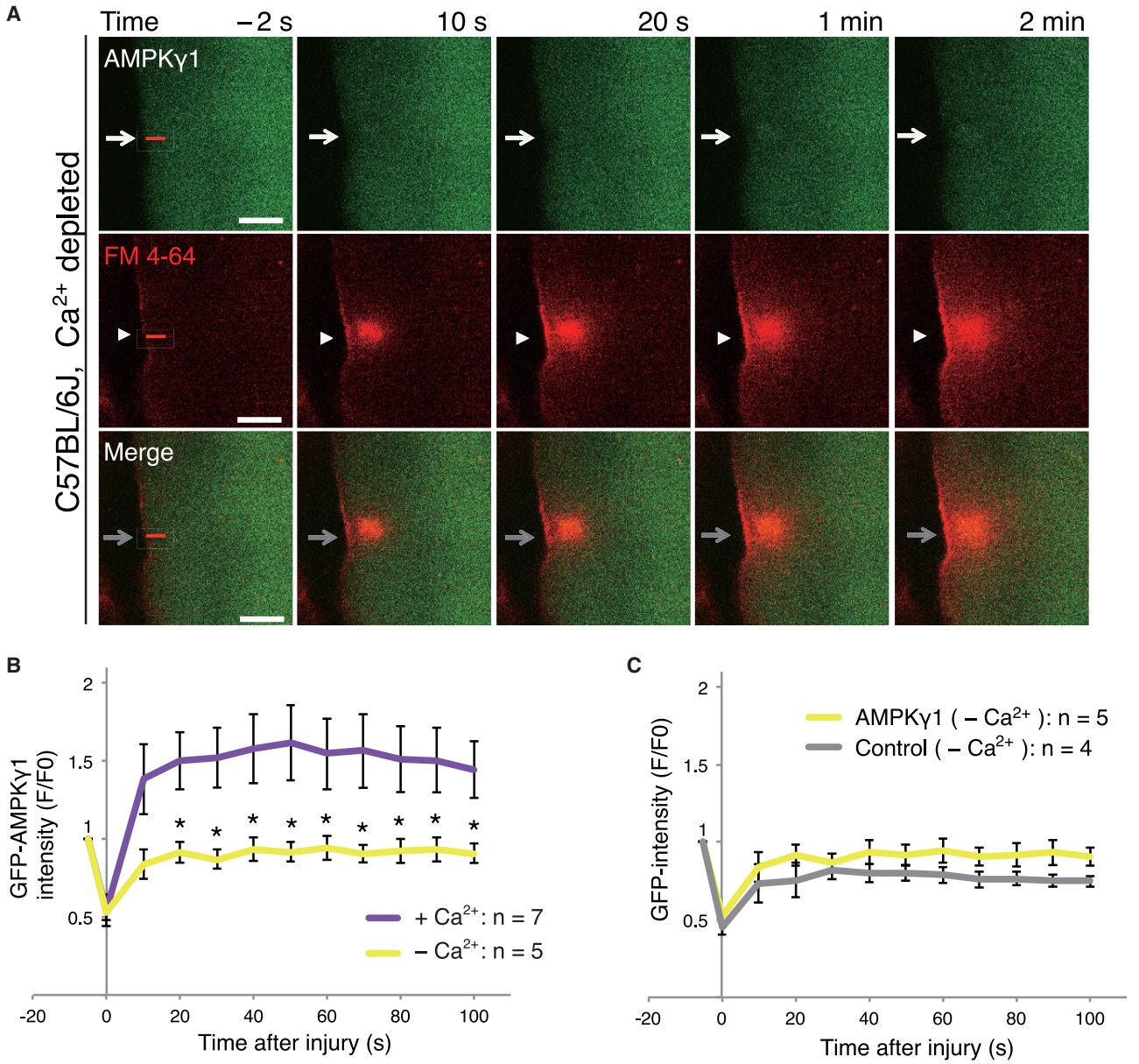

Figure 4. Injury-Triggered Accumulation of AMPKγ1 Is Dependent on the Presence of Ca^{2+}

(A) Isolated FDB muscle fibers from C57BL/6J mice expressing fluorescently tagged GFP-AMPKγ1 protein were injured (injured site, red line/arrow at −2 s) using a pulsed laser in the presence of FM4-64 fluorescent dye in a medium supplemented with 5 mM EGTA. The white arrows show the location of the damaged membrane. The injury site is indicated by FM4-64 accumulation (white arrowheads). Scale bars, 10 μm. (B) Quantification of the GFP-AMPKγ1 signal revealed an absence of increased fluorescence when Ca^{2+} was depleted. The data of fluorescence intensity of the GFP-AMPKγ1 in the C57BL/6J myofibers with Ca^{2+} abundance (+ Ca^{2+}) in Figure 2B were reused. + Ca^{2+} (Ca^{2+} abundance), n = 7 myofibers from four C57BL/6J mice; – Ca^{2+} (Ca^{2+} depletion), n = 5 myofibers from three C57BL/6J mice. (C) Without Ca^{2+}, no significant differences in fluorescence intensity were found between the GFP-AMPKγ1 signal and the unconjugated GFP signal (control) at the site of injury. The data of fluorescence intensity of the GFP-AMPKγ1 in the C57BL/6J myofibers with Ca^{2+} depletion (– Ca^{2+}) in (B) were reused. GFP-AMPKγ1, n = 5 myofibers from three C57BL/6J mice; control (unconjugated GFP), n = 4 myofibers from two C57BL/6J mice. Statistically significant differences (*$p < 0.05$) were determined using the Wilcoxon test. Data are expressed as mean ± SE.

results revealed a decrease in the protein level of dysferlin in line 107 (Figures S8A–S8C) and membrane-repair deficits compared with that in the control (Figure S8D). Following serum starvation and treatment with 5-aminoimidazole-4-carboxamide ribonucleotide (AICAR), an activator of AMPK, elevated levels of phosphorylated AMPK was observed in line 107 (Figures 6A and 6B). Surprisingly, treatment with AICAR significantly reduced the entry of the FM1-43 fluorescent dye into the myotubes of a patient with dysferlinopathy

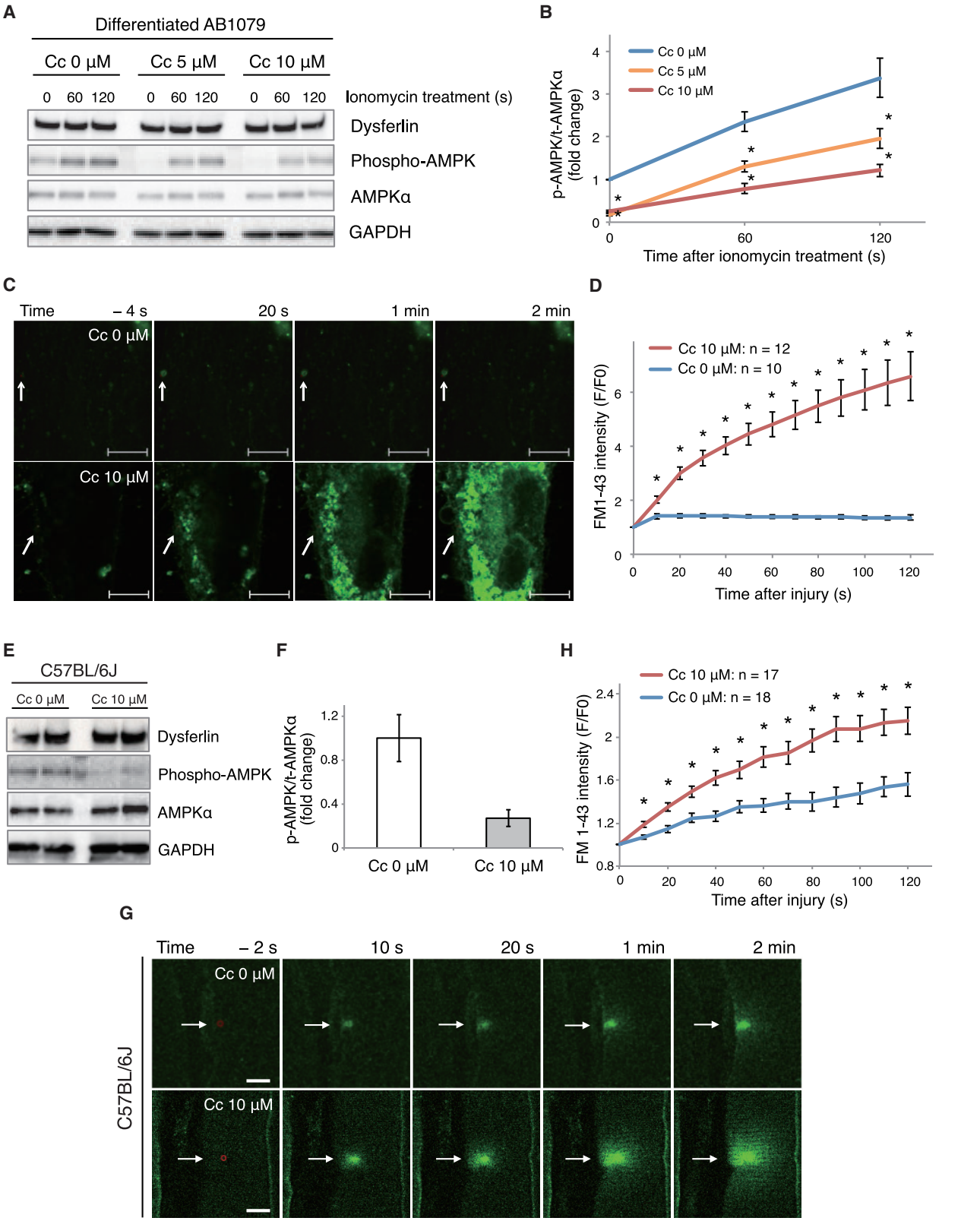

(legend on next page)

following laser-induced damage (Figures 6C and 6D; Videos S7 and S8). To determine whether treatment with an AMPK activator other than AICAR could rescue the membrane-repair defect, line 107 was treated with metformin, a drug used for the treatment of type 2 diabetes. As with AICAR, metformin increased the level of phosphorylated AMPK (Figures 6A and 6B) and rescued the membrane-repair defect (Figure 6E). AICAR also accelerated the membrane-repair process in immortalized human myotubes from normal subjects (AB1079) expressing normal levels of dysferlin (Figures S9A–S9C). However, in another patient with dysferlinopathy ("line 379") with complete dysferlin deficiency (Figures S10A–S10C), AICAR did not have an effect on membrane repair (Figures S10D–S10F). Finally, to evaluate the effect of AMPK activators using dysferlin-deficient mouse muscles, myofibers of BLA/J mice were used. The phosphorylation of AMPKα was compared between BLA/J mice myofibers treated with AICAR and those separately treated with phosphate-buffered saline (PBS) (+), and it was confirmed that the levels of phosphorylated AMPKα were elevated in the BLA/J mice myofibers treated with AICAR (Figures 6F and 6G). It was evident that AICAR treatment significantly reduced the entry of FM1-43 fluorescent dye into the myofibers of BLA/J mice following laser-induced damage (Figures 6H and 6I).

Zebrafish Model of Dysferlin Deficiency

The results of our *in vitro* studies indicated that AMPK activators increased membrane damage repair in the presence of dysferlin, even when the expression of dysferlin was low. To confirm the effect of an AMPK activator *in viv*o, the dysferlin-deficient zebrafish model was used.

The predicted amino acid sequence of zebrafish dysferlin has a similarity of approximately 68% to mammalian dysferlin. The N-terminal region of the predicted amino acid sequence is similar to those of human dysferlin variant 8 (GenBank: NM_003494) and mouse dysferlin variant 2 (GenBank: NM_001077694).[29] To generate zebrafish models of myopathies associated with dysferlin deficiency, a morpholino oligonucleotide (MO) was designed to disrupt the splicing pattern of *dysferlin* mRNA at the intron 3/exon 4 junction during development (Figure 7A). The injected embryos were examined 4 days post-fertilization (dpf). RT-PCR and sequence analyses confirmed that MO injection resulted in the complete deletion of *dysferlin* exon 4 (106 bp) (Figure 7B).

MO injection (1.5 ng) led to the loss of muscle birefringence (Figure 7C). To improve visualization of the structure and organization of morphant muscle fibers, the MO- and control MO (CMO)-injected embryos were analyzed using birefringence assays at 4 dpf (Figure 7C). The patterns of birefringence in the dysferlin morphant embryos were markedly abnormal compared with those in the WT and CMO embryos (Figures 7C and 7D). Of the MO-injected embryos, approximately 30.0% exhibited reduced birefringence, 36.7% appeared normal, and 33.3% had died (Figure 7D). The injection of increased doses of MO (3 or 6 ng) resulted in a dose-dependent increase in the percentage of dead fish. However, this percentage was unchanged among fish injected with 1, 3, or 6 ng of CMO (Figure S11). These findings indicate that the toxicity of these MOs was low.

AMPK Activators Improve Muscle Phenotype in a Zebrafish Model of Dysferlin Deficiency

Mixed populations of the above-mentioned morphants, which include normal, reduced birefringence, and dead fish, were used to confirm the effects of AMPK activators. We evaluated the percentage of reduced birefringence as a readout. It was found that AICAR treatment at 0.1, 1.0, and 10 mM increased the phosphorylation of AMPK, although this was not statistically significant between the AICAR-treated and untreated morphants (Figure 7E). Without AICAR treatment, 31.1% of the morphants exhibited abnormal birefringence (Figure 7F). Reduced birefringence was observed in 22.2%, 17.8%, and 17.8% of the fish administered with 0.1, 1.0, and 10 mM AICAR, respectively (Figure 7F). It was also confirmed that metformin treatment (1 and 10 mM) increased the phosphorylation of AMPK, although this was not statistically significant between the metformin-treated and untreated morphants (Figure 7G). Without metformin treatment, 33.3% of the morphants exhibited abnormal birefringence (Figure 7H). Metformin treatment reduced the percentage of affected fish exhibiting abnormal birefringence. Furthermore, reduced birefringence was observed in 25.0% and 20.8% of the fish administered with 1 and 10 mM metformin, respectively (Figure 7H). It was suggested that several AMPK activators improved the muscle phenotype in a zebrafish model of dysferlin deficiency.

AMPK Activator Improves the Muscle Phenotype in a Mouse Model of Dysferlin Deficiency

The effects of AMPK activators were investigated in well-studied mouse models of dysferlinopathy in BLA/J and SJL/J mice (Figure 8;

Figure 5. AMPKα Phosphorylation Is Important for Efficient Plasma Membrane Repair

(A) Western blot analysis of phospho-AMPKα in ionomycin-treated (0, 60, and 120 s after treatment) normal human skeletal muscle myotubes (AB1079) with or without compound C (Cc, a selective AMPK inhibitor). (B) Quantification of phospho-AMPKα expression normalized to total-AMPKα. Phospho-AMPKα increased after ionomycin administration. The basal activity of AMPKα phosphorylation was suppressed by Cc administration. Statistically significant differences (*$p < 0.05$) were determined using the Wilcoxon test. Data are expressed as mean ± SE. (C) Cc administration increased the influx of FM1-43 after laser injury of human myotubes. The arrows indicate the location of the damaged membrane. Scale bars, 10 μm. (D) Plot showing cell membrane-repair kinetics monitored by FM1-43 intensity. Cc 0 μM, n = 10 cells (10 experiments); Cc 10 μM, n = 12 cells (12 experiments). Statistically significant differences (*$p < 0.05$) were determined using the Wilcoxon test. Data are expressed as mean ± SE. (E) Western blot analysis of phospho-AMPKα in C57BL/6J mice myofibers with or without Cc administration. (F) Quantification of phospho-AMPKα expression normalized to total-AMPKα. Phospho-AMPKα was suppressed by Cc administration. Data are expressed as mean ± SE. (G) Cc administration increased the influx of the FM1-43 fluorescent dye after laser-induced injury of C57BL/6J mice myofibers. The arrows indicate the location of the damaged membrane. Scale bars, 10 μm. (H) Plot showing cell membrane-repair kinetics monitored by FM1-43 intensity. Cc 0 μM, n = 18 myofibers (six experiments, two C57BL/6J mice); Cc 10 μM, n = 17 myofibers (four experiments, two C57BL/6J mice). Statistically significant differences (*$p < 0.05$) were determined using the Wilcoxon test. Data are expressed as mean ± SE.

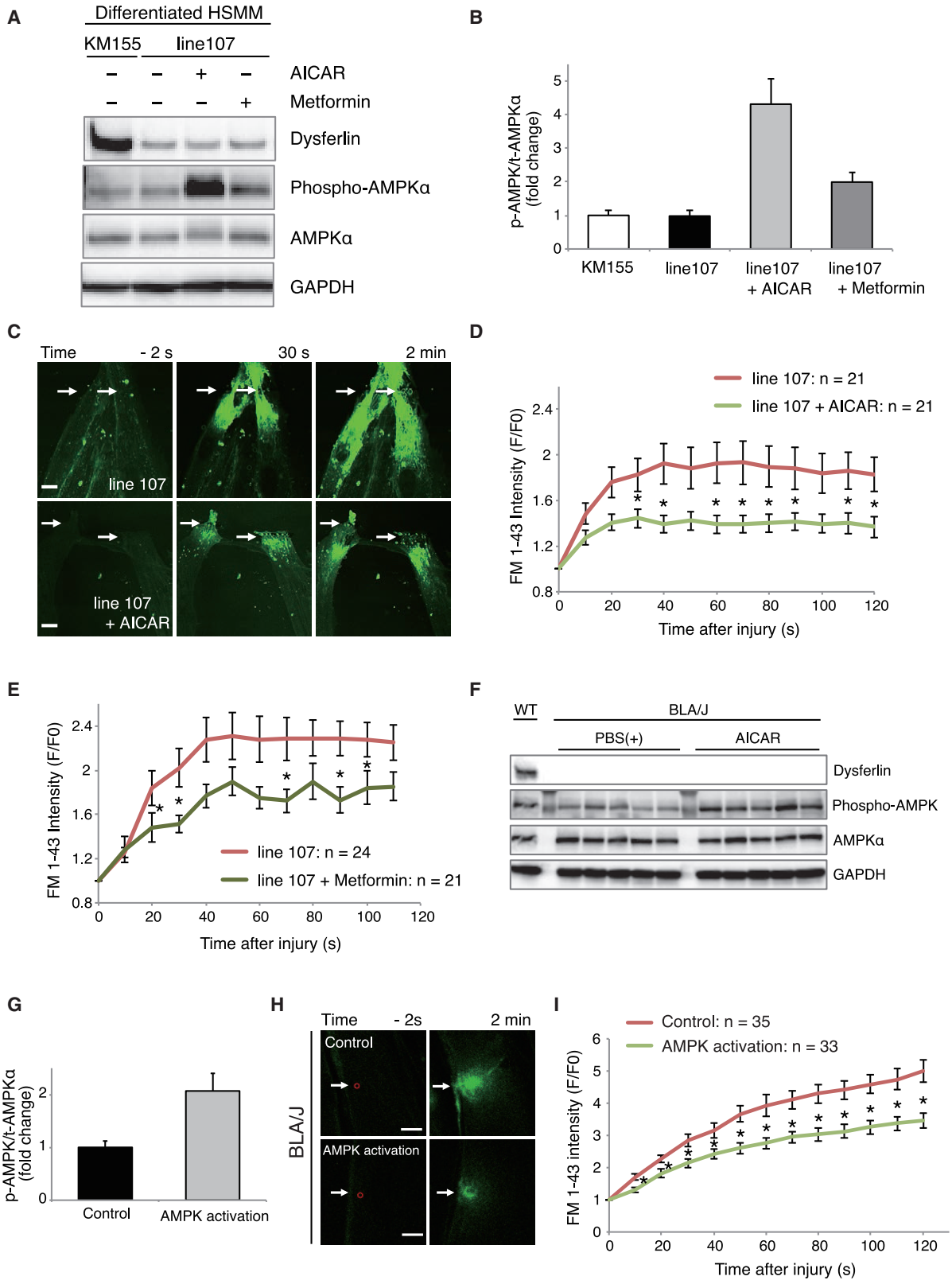

(legend on next page)

Figures S12–S14). A dysferlin defect was identified in BLA/J mice using immunoblotting (Figure S13). A previous study reported mouse plasma metformin concentrations of 0.45 and 1.7 μg/mL when administered in drinking water at concentrations of 1 and 5 mg/mL, respectively.[30] These plasma concentrations are similar to those in patients with diabetes treated with metformin (0.5–2.0 μg/mL). During 2 months, the activation of AMPK was compared between BLA/J mice treated with metformin and those untreated (Figure S12A). We addressed whether metformin treatment would be sufficient to modulate AMPK pathways in mice skeletal muscle. Acetyl-coenzyme A (CoA) carboxylase (ACC), a key enzyme in fatty acid synthesis, is the protein to be phosphorylated and inactivated by AMPK. Phosphorylation of ACC was usually indicated as the activity of the AMPK pathway.[31] Ribosomal protein S6 (S6) participates in the regulation of cell size, cell proliferation, and glucose homeostasis. Phosphorylation of S6 was decreased by AMPK activation.[32] Although the phosphorylation of AMPKα was variable across individual animals, long-term activation of AMPK and its downstream targets was observed following the oral administration of metformin (Figure S13). No reductions in animal body weight or grip strength were found during the experimental period (Figures S12B and S12C). The level of serum creatine kinase (CK) tended to decrease in the metformin-administered mice, although this was not statistically significant (Figure S12D). Muscle fiber histograms revealed a decrease in the severity of muscle atrophy and an increase in the number of normal muscle fibers (Figures S12E and S12F). The number of internal nuclei tended to decrease in the metformin-treated group (Figure S12G). In addition, to assess sarcolemmal membrane integrity, histological sections with fluorescent-labeled antibodies against mouse IgG were stained.[33] Quantification of the percentage of IgG-positive fibers tended to be lower in the metformin-treated mice, although this was not statistically significant (Figure S12H). Therefore, serum CK and histopathological analyses revealed that metformin treatment partially reduced myofiber damage in the BLA/J mouse model.

The second dysferlinopathy model in SJL/J mice was used following the observation of improved membrane repair in the partially deficient dysferlinopathy line (line 107) (Figure 6) but not in the completely deficient dysferlinopathy line (line 379) (Figure S10). The activation of AMPK was compared between SJL/J mice treated with metformin and those untreated for 8 months (Figure 8A). The long-term activation of AMPK and its downstream targets was observed following the oral (Figures S14A and S14B) and intraperitoneal (Figures S14C and S14D) administration of metformin. As with the results in the BLA/J mice, the levels of phosphorylated AMPKα were also variable. No reduction in the body weight was recorded during the experimental period (Figure 8B), whereas grip strength increased marginally in the metformin-treated mice (Figure 8C). It was also observed that the serum CK levels were significantly decreased in the metformin-treated mice (Figure 8D). Fibrosis was measured as the concentration of collagen (hydroxyproline) in gastrocnemius muscle tissues. Although no statistically significant difference in fibrosis was observed between the metformin-treated and control mice, the collagen concentrations tended to be lower in the metformin-treated mice (Figure 8E). Hematoxylin and eosin (H&E) images of muscle cross-sections are shown in Figure 8F. Decreased numbers of internal nuclei were also observed in the metformin-treated group (Figure 8G). Muscle fiber histograms revealed a significant decrease in the severity of muscle atrophy and an increase in the number of normal muscle fibers in the metformin-treated mice (Figures 8H and 8I). IgG staining images of the muscles in

Figure 6. AMPK Activators Rescue Membrane-Repair Defects in Immortalized Myotubes from a Patient with Dysferlinopathy and Dysferlin-Deficient Mouse Skeletal Muscle Fibers

(A) Line 107 with dysferlin mutations and the healthy control line KM 155 were used to examine the effects of serum starvation and AICAR or metformin treatment. AICAR treatment, 1 h at 1 mM; metformin treatment, 8 h at 2 mM. A representative western blot image of dysferlin, phospho-AMPK, AMPKα, and GAPDH in KM 155 and line 107 is shown. (B) Quantification of the average phospho-AMPK expression normalized to AMPKα from three independent experiments using KM 155, line 107, line 107 treated with AICAR, and line 107 treated with metformin. (C) Representative images of decreased FM1-43 fluorescent dye entry into AICAR-treated dysferlinopathy myotubes (line 107) following laser-induced damage. Scale bars, 10 μm. (D) AICAR treatment significantly reduced FM1-43 fluorescent dye entry into the dysferlinopathy myotubes (line 107) following laser-induced damage; line 107 + AICAR, n = 21 myotubes (six experiments); line 107, n = 21 myotubes (six experiments). Statistically significant differences (*$p < 0.05$) were determined using the Wilcoxon test. Data are expressed as mean ± SE. (E) Metformin treatment significantly reduced FM1-43 fluorescent dye entry into the dysferlinopathy line 107 myotubes following laser-induced damage; line 107 + metformin, n = 21 myotubes (six experiments); line 107, n = 24 myotubes (five experiments). Statistically significant differences (*$p < 0.05$) were determined using the Wilcoxon test. Data are expressed as mean ± SE. (F) FDBs of BLA/J mice were used to examine the effects of AICAR treatment. A previous study reported that the levels of phosphorylated AMPKα in mouse skeletal muscle at 20–40 min post-AICAR (250 mg/kg) injection were significantly higher than those at other time periods.[28] To leverage that work, AICAR (250 mg/kg) was injected into BLA/J mice intraperitoneally, and FDBs were isolated 20 min after injection. To achieve AMPK activation, the FDBs were cultured for 20 min in the presence of AICAR (2 mM) after isolation (labeled with AICAR). In the control group, the FDBs were cultured for 40 min in a PBS (+) buffer following isolation (labeled with PBS (+)). A representative western blot image of dysferlin, phospho-AMPK, AMPKα, and GAPDH in PBS (+) and AICAR is shown. (G) Quantification of phospho-AMPK expression was normalized to AMPKα. PBS (+) (control), n = 5 mice per cohort; AICAR (AMPK activation), n = 5 mice per cohort. Data are expressed as mean ± SE. (H) To achieve AMPK activation, the FDBs were cultured in the presence of AICAR (2 mM) after isolation. Membrane-repair assays were performed between 20 and 40 min after the intraperitoneal injection of AICAR (labeled with AMPK activation). In the control group, the FDBs were cultured for 40 min in a PBS (+) buffer following isolation. Membrane-repair assays were performed between 60 and 80 min after AICAR was administered (labeled with control). Representative images of decreased FM1-43 fluorescent dye entry into AICAR-treated BLA/J mouse FDB myofibers (AMPK activation) compared with PBS (+)-treated BLA/J mouse FDB myofibers (Control) following laser-induced damage are shown. Scale bars, 10 μm. (I) AMPK activation significantly reduced FM1-43 fluorescent dye entry into BLA/J mouse FDB myofibers following laser-induced damage. Control, n = 35 myofibers (10 experiments, five mice); AMPK activation, n = 33 myofibers (9 experiments, five mice). Statistically significant differences (*$p < 0.05$) were determined using the Wilcoxon test. Data are expressed as mean ± SE.

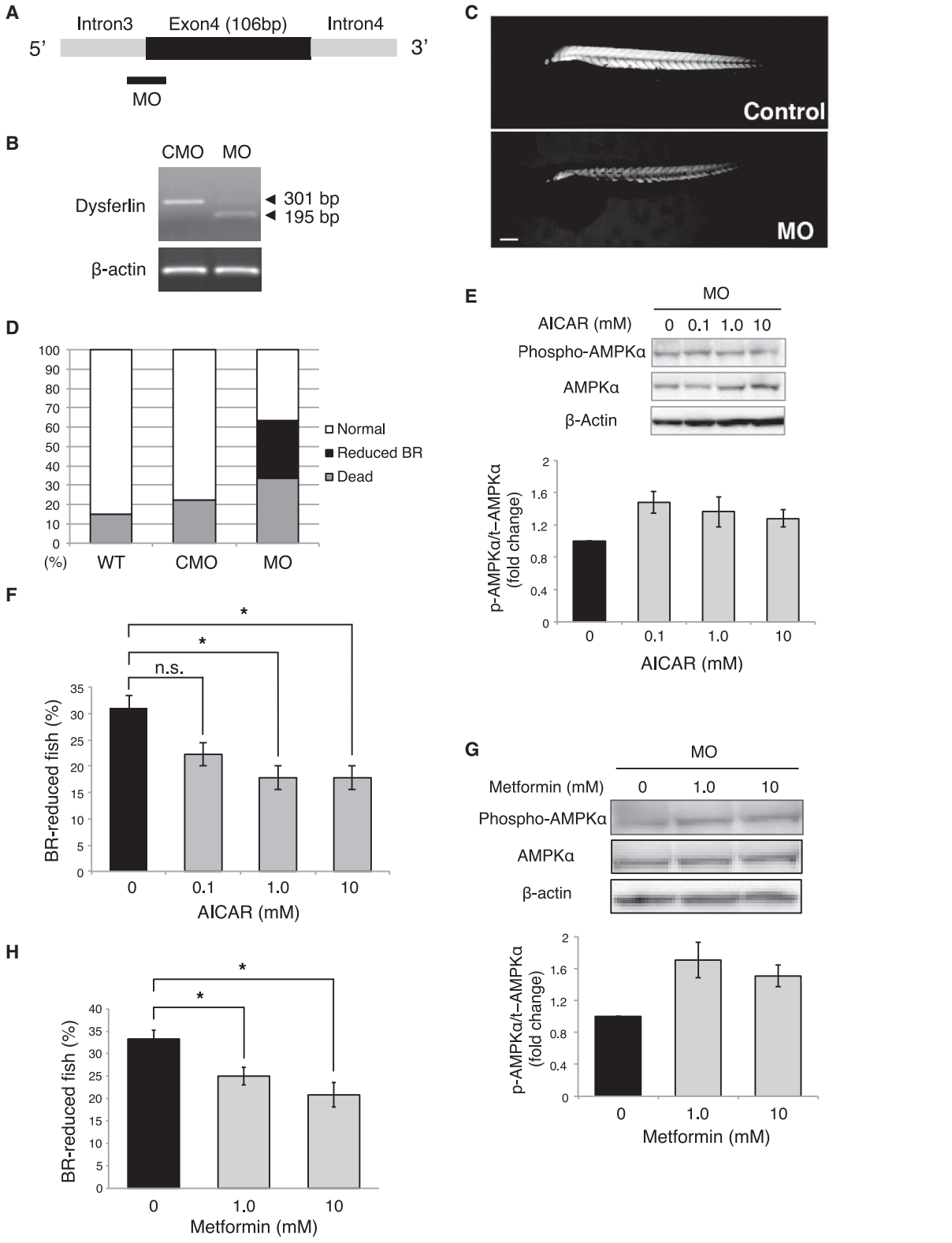

(legend on next page)

cross-sections are shown in Figure 8J. Quantification of the percentage of IgG-positive fibers was significantly lower in the metformin-treated mice (Figure 8K). These data indicate that the administration of metformin reduced muscle damage in the dysferlinopathy model.

DISCUSSION

We hypothesized that the binding partners of dysferlin serve as functional molecules during the membrane-repair process. The present study focused on the mechanisms underlying the interaction of dysferlin with several specific partners. As two Fer and DysF functional domains are situated between the third and fourth C2 domains, the binding protein at this site (II region) was examined via a biochemical approach (Figure 1A). Using recombinant proteins and affinity purification methods combined with LC-MS/MS, AMPKγ1 was shown to bind to dysferlin at the II region. AMPK is a critical regulator of skeletal muscle metabolism, transcription, and phenotype.[34] The potential for clinical synergism between the pharmacological and physiological stimulation of AMPK to ameliorate dystrophic pathology is particularly intriguing.[35,36] The AMPK complex is allosterically activated by increasing the concentrations of AMP and ADP, and via Thr172 residue phosphorylation on the α subunit.[37] The phosphorylated Thr172 residue can be dephosphorylated by three AMPK phosphatases: PPP1, PPP2A, and PPP2C.[37] As AMPKγ1 and PPP1CA were identified in dysferlin co-precipitates (Figure 1C), we examined whether the AMPK complex is involved in dysferlin function and membrane repair. The results revealed for the first time that the AMPK complex is involved in the membrane-repair process.

AMPK consists of a heterotrimeric protein complex containing a catalytic α subunit and two regulatory subunits (β and γ) in the stoichiometry of 1α:1β:1γ.[34] The seven AMPK subunit isoforms give rise to 12 heterotrimeric combinations that appear to be expressed in a tissue-specific manner. In skeletal muscle preparations from humans and mice, all subunit isoforms have been detected, but only a subset of possible heterotrimeric complexes appears to exist.[38,39] In human skeletal muscle (*vastus lateralis*), three different complexes have been described (α2β2γ1, α2β2γ3, and α1β1γ1),[38] whereas in mouse skeletal muscle, five complexes have been identified (α2β2γ1, α2β2γ3, α2β1γ1, α1β2γ1, and α1β1γ1).[39] In addition, certain AMPK subunits are expressed in a fiber-dependent manner,[40] which may explain the relative distribution of complexes between different muscles.[39] Among these AMPK subunit isoforms, we found that the AMPK complex (comprising γ1 and α1) is required for effective membrane repair in C2C12 cells (Figure 3).

Despite the numerous downstream targets of the AMPK complex,[41,42] its direct involvement in plasma membrane repair remains to be elucidated. The targeted disruption of the mouse AMPKγ1 gene causes regenerative hemolytic anemia by increasing the sequestration of abnormal erythrocytes.[43] AMPKγ1-deficient erythrocytes are highly resistant to osmotic hemolysis and are poorly deformable in response to increasing shear stress, consistent with greater membrane rigidity.[43] These observations suggest that the AMPK complex is also involved in the maintenance of plasma membrane integrity in non-muscle cells. Our *ex vivo* laser injury experiments revealed the importance of the AMPK complex for membrane repair of sarcolemmal damage in skeletal muscle fibers. We now know that AMPK complex accumulation in response to injury is dependent on the presence of Ca^{2+}, and the rate of this accumulation is regulated by dysferlin. Dysferlin is considered to interact with MG53, annexins, and other proteins during vesicle accumulation at the site of injury following membrane disruption.[16,17,44] Annexins (A1, A2, A5, and A6) form a repair cap at the membrane lesion,[45] whereas the AMPK complex is recruited either to the site of injury (Figures S6B, S6C, and S7A) or to surrounding the site of injury (Figure 2A; Figures S5A and S6A), similar to MG53.[20] Elucidating the involvement of the AMPK complex with these proteins during muscle membrane repair is required.

The novel schema we propose suggests that the membrane-repair process is associated with dysferlin and the AMPK complex. Membrane disruption causes Ca^{2+} flooding into the muscle fiber and creates a high Ca^{2+} zone around the disruption site. The ability of the ferlin C2 domains to bind phospholipids in a Ca^{2+}-sensitive manner has been suggested.[46] High Ca^{2+} levels result in the binding of the

Figure 7. AICAR and Metformin Treatment Improve the Muscle Phenotype in a Zebrafish Model of Dysferlin Deficiency

(A) Morpholino oligonucleotides (MOs) targeting zebrafish dysferlin. (B) A single RT-PCR product of 301 bp was seen in 4-dpf embryos injected with 1.5 ng of control MO; two differently sized RT-PCR products of 301 and 195 bp were seen in 4-dpf embryos injected with 1.5 ng of dysferlin. (C) Panels represent the results of the birefringence assay (BR). The abnormal structure of the muscles is more clearly seen in dysferlin MO-injected fish (MO, lower panel) than in controls (CMO, upper panel) under BR. Scale bar, 200 μm. (D) Histogram of the percentage of normal, affected (reduced BR), and dead fish upon MO injection. After injecting 1.5 ng of MO, approximately 30.0% of the embryos exhibited reduced birefringence. The white, black, and gray bars show the percentage of normal, reduced BR, and dead fish, respectively. WT, uninjected fish; CMO, CMO-injected fish; MO, MO-injected fish. (E) Representative western blot image of phospho-AMPK, AMPKα, and β-actin in MO-injected fish treated with AICAR for 4 days at 0, 0.1, 1.0, or 10 mM. Quantification of phospho-AMPK expression was normalized to AMPKα in the lower panels. (F) AICAR treatment reduced the percentage of BR-reduced fish. Results for metformin concentrations of 0, 0.1, 1.0, and 10 mM are the average of three independent experiments. Of the untreated MO morphants, 31.1% were BR reduced. AICAR treatment at concentrations of 0.1, 1.0, and 10 mM reduced the percentage of BR-reduced fish to 22.2%, 17.8%, and 17.8%, respectively. Statistically significant differences were determined using ANOVA followed by Tukey's multiple comparisons test. Statistical significance was set at $^*p < 0.05$. (G) Representative western blot image of phospho-AMPK, AMPKα, and β-actin in MO-injected fish treated with metformin for 4 days at 0, 1, and 10 mM. Quantification of phospho-AMPK expression was normalized to AMPKα in the lower panels. Results for metformin concentrations of 0, 1, and 10 mM are the average of three independent experiments and were normalized to those without metformin treatment. (H) Metformin treatment reduced the percentage of BR-reduced fish. Results for metformin concentrations of 0, 1, and 10 mM are the average of three independent experiments. Of the untreated MO morphants, 33.3% were BR-reduced fish. Metformin treatment at concentrations of 1 and 10 mM reduced the percentage of BR-reduced fish to 25.0% and 20.8%, respectively. Statistically significant differences were determined using ANOVA followed by Tukey's multiple comparisons test. Statistical significance was set at $^*p < 0.05$.

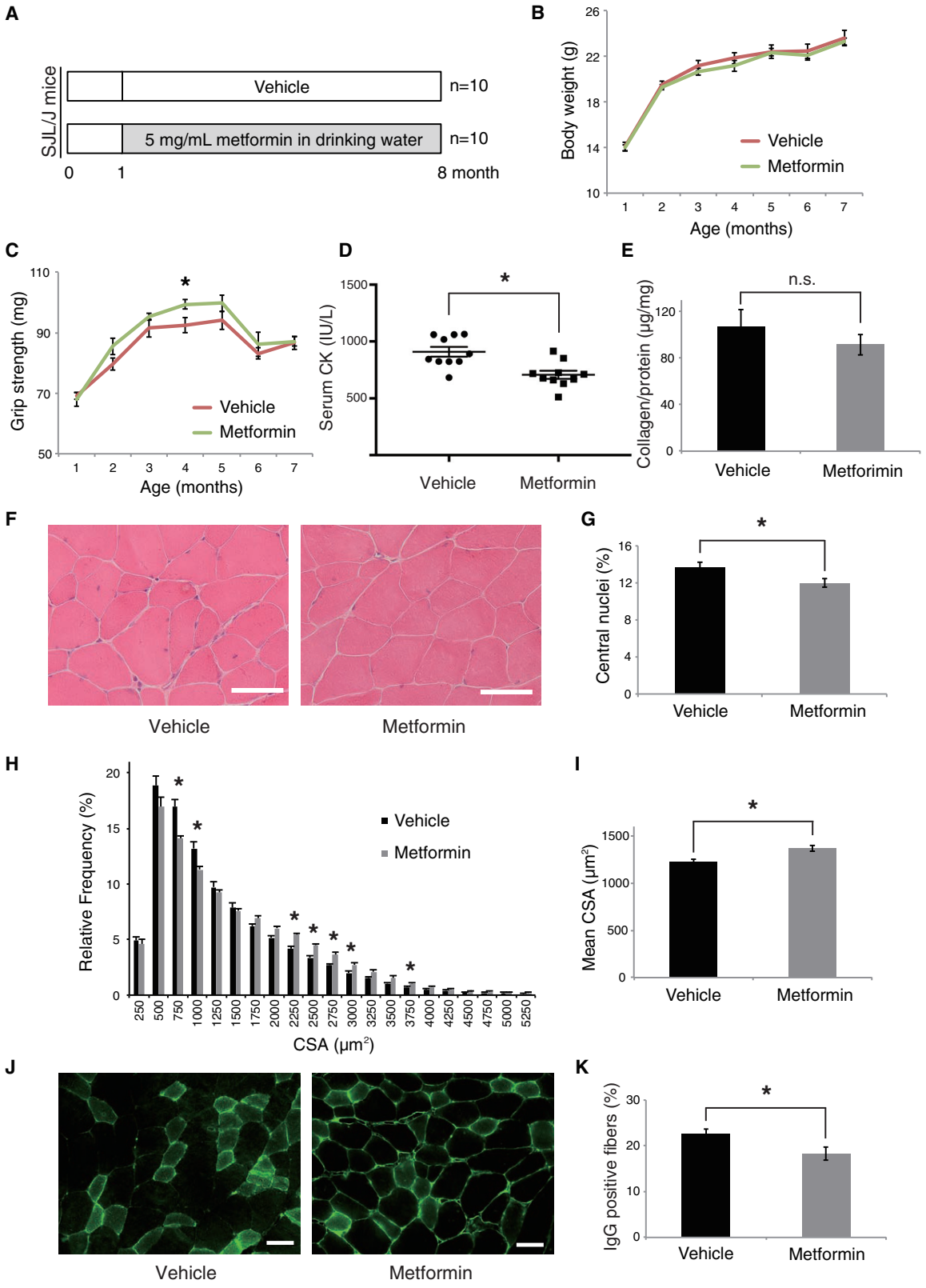

(legend on next page)

dysferlin C2 domain to sarcolemmal phospholipids, thereby presumably causing structural changes in the II region of dysferlin. Ca^{2+} flux also results in the phosphorylation of AMPKα (Figures 5A and 5B). Our results suggest that a conformational change in the II region triggers the interaction between dysferlin and the AMPK complex, because the co-localization of dysferlin and the AMPK complex primarily occurred with membrane damage (Figure 2C; Figures S3 and S4). It should be appreciated that one limitation of this method is its reliance on the overexpression of fluorescently-tagged proteins. Visualizing the conformational change of dysferlin by a Ca^{2+} flux via a nano-dynamics visualization technique, such as high-speed atomic force microscopy,[47,48] may assist in proving this hypothesis.

We observed that membrane repair was improved in a partially deficient dysferlinopathy line (line 107) by the phosphorylation of AMPKα (Figures 6A–6E) but not in a completely deficient dysferlinopathy line (line 379, Figure S10). This suggested that the dysferlin-AMPK complex is actively involved in membrane repair. Conversely, it was observed that GFP-AMPKγ1 was recruited to the wound even in the complete absence of dysferlin in mice, although at a slower rate in this context (Figures 2E and 2F). Additionally, AICAR treatment significantly reduced the entry of the FM1-43 fluorescent dye into the myofibers of BLA/J mice following laser-induced damage (Figures 6H and 6I). These findings demonstrate that the dysferlin-independent pathway for the regulation of AMPK phosphorylation is also involved in membrane repair in dysferlinopathy.

Interestingly, animal models with AMPK depletion, specifically in skeletal muscle fibers, exhibit a myopathic phenotype.[49–51] In the muscles of young and old mice, a low-calorie diet activates AMPK and markedly increases muscle regeneration.[52] The results of several studies in which dystrophin-deficient *mdx* mice were treated with AMPK activation compounds, such as AICAR, resveratrol, and metformin, suggest that targeting AMPK in the skeletal muscle may ameliorate the pathology observed in patients with Duchenne muscular dystrophy (DMD).[53–55] We examined three types of *in vivo* dysferlin-deficient models. In the case of MO-administered zebrafish, a small amount of dysferlin transcript persisted (Figure 7B). SJL/J mice had approximately 15% residual dysferlin (Figure S14A), whereas BLA/J mice had no dysferlin (Figure S13A). We found that the activation of AMPK improved membrane repair in dysferlin-deficient mouse muscle fibers (BLA/J mice, Figures 6F–6I), and treatment with metformin partially reduced muscle damage in BLA/J mice (Figure S12). Additionally, activation of the dysferlin-AMPK complex markedly improved membrane repair (line 107; Figures 6A–6E) and the muscle phenotype in zebrafish (Figure 7) and SJL/J mice (Figure 8), exhibiting with residual expression of dysferlin. Therefore, utilization of the protein-protein interaction of AMPK with dysferlin for developing a therapeutic strategy in patients with dysferlinopathy is important. Nonsense suppression drugs, such as ataluren,[22] which increases the expression of dysferlin in patients with dysferlinopathy, may be useful in establishing an effective combination therapy. Previous studies have reported that promoting sarcolemmal repair via a glucocorticoid steroid regimen improved muscle function in several muscular dystrophy mouse models, such as DMD, LGMD 2B, and LGMD 2C (caused by mutations in the gene encoding sarcoglycan).[56,57] The novel concept of the dysferlin-AMPK complex involved in the plasma membrane-repair process may contribute to drug development for several types of muscular dystrophy.

A limitation of this study lies in the *in vivo* experiments, specifically in zebrafish and mice. Because AMPKα phosphorylation was variable across individual animals, there was no significant increase in the AMPKα phosphorylation. The variations between individual samples can be explained by the previous observation that AMPK in fish can be activated by metformin[58] and exercise[59] and that AMPK in mouse skeletal muscle can be activated by metformin[60,61] and exercise.[62,28] In this study, metformin in drinking water was administered to dysferlin-deficient mice from a drug-repositioning perspective. AMPK plays a role in energy homeostasis in not only skeletal muscles but also a number of tissues, such as liver, pancreas, and brain.[63] It is necessary to consider a drug delivery system or genomic drug discovery (development of medicines using information about human genome) for muscle-specific AMPKα phosphorylation.

Overall, these results indicate a functional association between dysferlin and the AMPK-linked signaling pathways. Furthermore, this study sheds light on a new dimension of dysferlin as a membrane scaffold protein for several functional proteins. Further identification of the numerous molecules that form complexes with dysferlin is important for understanding the whole landscape of plasma membrane repair and developing novel therapeutic targets.

Figure 8. Eight Months of Metformin Treatment Ameliorated the Aberrant Phenotype of Dysferlin Mutant SJL/J Mice

(A) Protocol: 5 mg/mL metformin in drinking water was administered to SJL mice aged 1–8 months (n = 10 each). (B) Body weight during the experimental period. Vehicle, n = 8 mice per cohort; metformin, n = 10 mice per cohort. (C) Grip strength during the experimental period. Vehicle, n = 8 mice per cohort; metformin, n = 10 mice per cohort. Statistically significant differences (*$p < 0.05$) were determined using the Wilcoxon test. (D) Metformin regimens comparably reduced serum CK at 8 months. Vehicle, n = 8 mice per cohort; metformin, n = 10 mice per cohort. (E) Quantification of the collagen content (collagen/protein ratios) in gastrocnemius muscle tissue. Metformin regimens tended to decrease collagen content as compared with vehicle treatment. Vehicle, n = 8 mice per cohort; metformin, n = 10 mice per cohort. (F) Representative H&E staining images of gastrocnemius muscle. Scale bars, 50 μm. (G) Metformin treatment decreased the number of internal nuclei in the gastrocnemius muscle sections. Vehicle, 1,960 fibers from n = 8 mice; metformin, 2,403 fibers from n = 10 mice per cohort. (H) Histogram of cross-sectional analysis (CSA) of the gastrocnemius muscle. The CSA was examined by comparing the individual histograms. Vehicle, 41,405 fibers from n = 8 mice; metformin, 48,388 fibers from n = 10 mice. Statistically significant differences (*$p < 0.05$) were determined using the Wilcoxon test. (I) Metformin treatment increased CSA in the gastrocnemius muscle sections. Vehicle, n = 8 mice per cohort; metformin, n = 10 mice per cohort. (J) Representative IgG staining images of gastrocnemius muscle. Scale bars, 50 μm. (K) Metformin treatment decreased the percentage of IgG-positive fibers in the gastrocnemius muscle sections. Vehicle, 2,571 fibers from n = 8 mice; metformin, 2,722 fibers from n = 10 mice. Statistically significant differences (*$p < 0.05$) were determined using the Wilcoxon test.

MATERIALS AND METHODS

All protocols were approved by the Ethics Committees of the Tohoku University School of Medicine (nos. 2014-208 and 2018-196 for genetics; nos. 2014-216, 2015-170, and 2018-247 for animals).

Cell Culture

Mouse C2C12 myoblasts (American Type Culture Collection, Manassas, VA, USA) were routinely cultured in Dulbecco's modified Eagle's medium (DMEM) with high glucose (FUJIFILM Wako Pure Chemical, Osaka, Japan) supplemented with 10% fetal bovine serum (FBS; GE Healthcare, Chicago, IL, USA) at 37°C and 5% CO_2. HEK293T cells (American Type Culture Collection, Manassas, VA, USA) were cultured in RPMI 1640 (FUJIFILM Wako Pure Chemical, Osaka, Japan) containing 10% FBS. The immortalized myoblast lines used in this study are presented in Table S3. The immortalized dysferlin-deficient myoblast lines (line 107 and line 379) and control human myoblast lines (KM 155 and AB 1079) were cultured in growth medium comprising a 1:4 ratio (by volume) of Medium 199 (Thermo Fisher Scientific, Waltham, MA, USA) and DMEM supplemented with 20% FBS, 2.5 ng/mL hepatocyte growth factor (HGF) (Thermo Fisher Scientific, Waltham, MA, USA), 0.1 μM dexamethasone (Sigma-Aldrich, St. Louis, MO, USA), and 50 μg/mL gentamycin (Thermo Fisher Scientific, Waltham, MA, USA), as described in earlier reports.[27] Differentiation into myotubes was initiated at approximately 70%–80% confluence in DMEM with 2% horse serum (Thermo Fisher Scientific, Waltham, MA, USA).

Plasmid Construction

A human cDNA library was purchased from Takara Bio (Kusatsu, Japan). Amplified fragments of deletion mutants of *dysferlin* with additional *Sal*I or *Xho*I sites at the 5′ end and *Not*I sites at the 3′ end were cloned into MBP-tag and pEGFP-N1 vectors (Takara Bio, Kusatsu, Japan). The primers used in this study are presented in Table S1.

RNA Interference

RNA oligonucleotides were transfected into C2C12 myoblasts using Lipofectamine RNAiMAX transfection reagent (Thermo Fisher Scientific, Waltham, MA, USA), in accordance with the manufacturer's instructions. Briefly, siRNA and Lipofectamine reagent were separately diluted in Opti-MEM (Thermo Fisher Scientific, Waltham, MA, USA). The diluted Lipofectamine reagent was added to the siRNA mixture and allowed to form a complex with the siRNA for 10 min. The lipid/siRNA complexes were then added to the differentiation medium, and myoblasts were incubated for 24 h in the medium containing the transfection mixture. The final concentration of siRNA was set at 10 nM. The siRNA oligonucleotides used in this study are listed in Table S2.

Pull-Down Assay and Nano-LC-MS/MS

MBP-tagged DYSF-II, -II-1, and -II-2 were constructed in a pMAL vector (New England Biolabs, Ipswich, MA, USA) via PCR amplification and expressed in *E. coli.* Each cell lysate was incubated with amylose resin (50-mL volume; New England Biolabs, Ipswich, MA, USA) for 1 h at 4°C and washed twice with washing buffer A (50 mM Tris–HCl [pH 7.5], 0.3 M NaCl, and 0.1% Nonidet P-40 [NP-40]), twice with washing buffer B (50 mM Tris–HCl [pH 7.5] and 1.0 M NaCl), and once with PBS. HEK293 cell pellets (4 g) were extracted in 5 mL of extraction buffer (50 mM HEPES [*N*-2-hydroxyethylpiperazine-*N*′-2-ethanesulfonic acid] [pH 7.5], 0.3 M NaCl, and 0.2% NP-40) by sonication, and the extracts were clarified by centrifugation at 12,000 rpm for 30 min at 4°C. A 50-mL volume of MBP-tagged DYSF-II, -II-1, and -II-2 amylose beads was incubated with 1.5 mL of HEK293T cell lysate for 4 h at 4°C. Following centrifugation for 2 min at 1,200 rpm, the beads were washed three times with washing buffer C (50 mM HEPES [pH 7.5], 0.15 M NaCl, and 0.2% NP-40) and eluted with 0.6 mL of elution buffer (50 mM HEPES [pH 7.5] and 1.2 M NaCl). The eluates were then concentrated down to 50 mL and desalinated by centrifugal filter devices (Amicon Ultra; Merck Millipore, Burlington, MA, USA), and 2× SDS sample buffer was added. The samples were resolved on a 4%–15% SDS-PAGE gel and stained using a Wako silver stain kit (FUJIFILM Wako Pure Chemical, Osaka, Japan). Gel slippage was decreased by 100 mM DTT and alkylated with 100 mM iodoacetamide. Following washing, the gels were incubated with trypsin overnight at 30°C. The recovered peptides were desalted in ZipTip C18 (Merck Millipore, Burlington, MA, USA). The samples were analyzed using nano-LC-MS/MS systems (DiNa HPLC [high-pressure liquid chromatography] system, Techno Alpha, Tokyo, Japan; QSTAR XL hybrid LC-MS/MS system, Thermo Fisher Scientific, Waltham, MA, USA). Mass data acquisitions were piloted using Mascot software.

Co-immunoprecipitation Assay

C57BL/6J mouse skeletal muscle samples (40 mg) were ground into powder with a mortar and pestle under the constant addition of liquid nitrogen. The powder was suspended in a 15× volume of ice-cold lysis/equilibration buffer (Takara Bio, Kusatsu, Japan) and centrifuged at 17,000 × *g* for 20 min. The supernatants were incubated with an appropriate antibody and protein A-Sepharose 4 Fast Flow (GE Healthcare, Chicago, IL, USA) for 1 h at 4°C with end-over-end rotation. The beads were washed with PBS three times and elution was performed in elution buffer (0.1 M glycine [pH 2.5]) with neutralization buffer (1 M Tris [pH 8.5]).

Immunoblotting

Equal quantities of protein (20-μg samples) were boiled, subjected to SDS-PAGE, and electrophoresed at 200 V for 1 h. The gels were transferred onto a polyvinylidene difluoride membrane (Merck Millipore, Burlington, MA, USA). The membranes were then blocked with 5% bovine serum albumin (BSA)/PBS and incubated with primary antibodies overnight at 4°C. The membranes were incubated with an anti-mouse (#7076; Cell Signaling Technology, Danvers, MA, USA) or anti-rabbit IgG horseradish peroxidase (HRP)-linked antibody (#7074; Cell Signaling Technology, Danvers, MA, USA) for 1 h. Immunodetection was performed using the ECL (enhanced chemiluminescence) Prime western blot analysis system (GE Healthcare, Chicago, IL, USA), and images were captured with an Omega Lum G (Gel Company, San Francisco, CA, USA), in accordance with the manufacturers' instructions.

Immunofluorescence

Frozen muscle sections were cut to a thickness of 10 μm, air-dried, and fixed in 4% paraformaldehyde. Following incubation with PBS containing 5% BSA, the sections were probed with primary antibodies. Following several washes with PBS, the sections were incubated with appropriate secondary antibodies for 1 h. The sections were mounted with a coverslip containing a drop of mounting medium (Vector Laboratories, Burlingame, CA, USA).

Antibodies

Antibodies against the following proteins were obtained from Cell Signaling Technology (Danvers, MA, USA): ACC (1:1,000 for immunoblotting, #3662), phosphorylated (phospho-)ACC (Ser79) (1:1,000 for immunoblotting, #3661), AMPKα (1:1,000 for immunoblotting, #2532S), AMPKα2 (1:1,000 for immunoblotting, #2757S), phospho-AMPK (Ser172) (1:1,000 for immunoblotting, #2531S), GAPDH (1:1,000 for immunoblotting, #2118), S6 (1:1,000 for immunoblotting, #2217), phospho-S6 (1:1,000 for immunoblotting, #4858), β-actin (1:1,000 for immunoblotting, #4967), and normal rabbit IgG (5 μg/sample for immunoprecipitation, #2729); from Abcam (Cambridge, UK): AMPKγ1 (1:1,000 for immunoblotting, 5 μg/sample, for immunoprecipitation, ab32508), AMPKα1 (1:1,000 for immunoblotting, 1:1,000 for immunofluorescence, ab3759), dysferlin (5 μg/sample for immunoprecipitation, ab214078), GFP (1:1,000 for immunoblotting, ab290), red fluorescent protein (RFP) (1:1,000 for immunoblotting, ab62341); from Leica Biosystems (Nussloch, Germany): dysferlin (1:250 for immunoblotting, NCL-Hamlet); from Sigma (St. Louis, MO): dysferlin (1:250 for immunofluorescense, HPA017071); and from Medical and Biological Laboratories (Nagoya, Japan): RFP (5 μg/sample for immunoprecipitation, M208-3).

Ionomycin and Cc treatment

In Vitro

The cells were cultured overnight in the presence or absence of serum and were treated with or without 1 μM ionomycin (FUJIFILM Wako Pure Chemical, Osaka, Japan). The cells were cultured overnight in the presence or absence of serum and were treated with or without the AMPK inhibitor Cc (Abcam, Cambridge, UK; 5 and 10 μM) for 1–4 h.

In Vivo

A total of 10 μL of Cc or saline was injected into the *flexor digitorum brevis* (FDB) of anesthetized, 3-month-old male C57BL/6J mice. Skeletal muscle myofibers were isolated 1 h after injection. The Cc-administered myofibers were cultured for 30 min in the presence of Cc (10 μM). The saline-administered myofibers were cultured for 30 min in the presence PBS (+).

AICAR and Metformin Treatment

In Vitro

The cells were cultured overnight in the presence or absence of serum and were left untreated or treated with the AMPK activator AICAR (Sigma, St. Louis, MO, USA; 1 mM, 1–9 h) and metformin (Sigma, St. Louis, MO, USA; 2 mM, 8–12 h) 7–10 days after the initiation of differentiation.

In Vivo

A previous study reported that the levels of phosphorylated AMPKα in mouse skeletal muscle at 20–40 min post-AICAR (250 mg/kg) injection were significantly higher than those at other time periods.[28] To leverage that work, AICAR (250 mg/kg) was injected into the anesthetized, 18-month-old male BLA/J mice intraperitoneally, and FDB was isolated 20 min after injection. Two goals were established. To achieve AMPK activation, the FDBs were cultured in the presence of AICAR (2 mM) after isolation. Membrane-repair assays were performed between 20 and 40 min after the intraperitoneal injection of AICAR. In the control group, the FDBs were cultured for 40 min in a PBS (+) buffer following isolation. Membrane-repair assays were performed between 60 and 80 min after AICAR was administered.

Membrane-Repair Assay

In Vivo *Transfection*

A total of 20 μg of Venus-tagged human dysferlin, DsRed-tagged human AMPKγ1, GFP-tagged human AMPKγ1, and AMPKα1/AMPKα2 were injected into the FDB of anesthetized, 3-month-old male C57BL/6J or BLA/J mice. Electroporation of the plasmid DNA was performed using an electric pulse generator (CUY21SC; Nepa Gene, Ichikawa, Japan). Skeletal muscle myocytes (for whole-mount viewing) or individual myofibers were isolated 14 days after the electroporation.

Membrane-Repair Assays

Membrane-repair assays were performed as described in a previous report.[8] Briefly, membrane damage was induced in the presence of the FM1-43 or FM4-64 dye (2.5 mM; Molecular Probes) using a two-photon confocal laser-scanning microscope with ×40 magnification and 1.2 numerical aperture (LSM710NLO; Zeiss, Oberkochen, Germany) coupled to a 10-W Argon/Ti:sapphire laser. A circular area (2–6 mm in diameter) in the injury site was selected along the edge of the sarcolemma and irradiated at 1.5 ± 0.2 mW, which was measured by a photodiode sensor (PD300-3W; Ophir Optronics, Jerusalem, Israel). Images were captured beginning at 20 s before (t = 0) and for 2–4 min after irradiation at 10-s intervals. For every image captured, the fluorescence intensity at the damage site was measured using Zeiss LSM 710NLO imaging software.

Zebrafish Experiments

Fish Culture

Zebrafish (the AB line) were cultured at 28.5°C in accordance with standard procedures and standard criteria.[64] Fertilized eggs were collected and used for injection. For anesthesia and euthanasia, tricaine solution was used.

MO Injections

An antisense MO targeted to disrupt the splicing of *dysferlin* mRNA was designed by Gene Tools (Philomath, OR, USA). The morpholino

sequence for *dysferlin* MO was 5′-CAGCATGGGAATAAACT CACCTGGT-3′. The morpholinos (1.5 ng) were injected into the yolk of one- to two-cell-stage embryos. For the injection control, CMO was used (standard control oligonucleotide; Gene Tools, Philomath, OR, USA): 5′-CCTCTTACCTCAGTTACAATTTAT-3′. To confirm the effect of the morpholino injections, zebrafish total RNA was extracted from embryos at 4 dpf using an RNeasy micro kit (QIAGEN, Hilden, Germany) and was converted to cDNA (SuperScript III; Thermo Fisher Scientific, Waltham, MA, USA). To detect misspliced products, PCR was performed with ExTaq DNA polymerase (Takara Bio, Kusatsu, Japan) at 95°C for 30 s, 55°C for 30 s, and 72°C for 30 s for 35 cycles with the following primer sets: *dysferlin* for exon 4, forward, 5′-GGACCTGAAGGGTGT TCCTT-3′, reverse, 5′-TGTGACTGTGTCCAGCTCCA-3′; and β-actin, forward, 5′-CGGTTTTGCTGGAGATGATG-3′, reverse, 5′-CGTGCTCAATGGGGTATTTG-3′.

Detection of Muscle Phenotype of Morphants by Birefringence

A birefringence assay was performed to detect abnormal skeletal muscle structures by placing anesthetized fish on a polarizing filter and subsequently covering them with a second polarizing filter.[65] The filters were placed on an underlit dissection scope and the top-polarizing filter was twisted until only the light refracting through the striated muscle was visible. Because the degree of birefringence is affected by the horizontal orientation of the fish, the fish were oscillated back and forth to account for differences in positioning.

Long-Term Mouse Experiments

All mice were handled according to the approved animal protocols of our institution. The gastrocnemius and tibialis anterior muscles were dissected from female SJL (SJL/JOrllcoCrj) mice (n = 20; Charles River Laboratories, Yokohama, Japan). Prior to this study, the muscles of both strains of mice were examined to investigate the muscular pathology and progression of myopathy.[66] BLA/J (B6.A-*Dysf*^{prmd}/GeneJ) mice were obtained from The Jackson Laboratory (Bar Harbor, ME, USA).

Metformin Administration Study

A total of 20 SJL/J mice were randomized to receive vehicle (n = 10) or 5 mg/mL metformin (n = 10), and 10 BLA/J mice were randomized to receive vehicle (n = 5) or 5 mg/mL metformin (n = 5).

Determination of CK Levels

Blood (10 μL) was collected in Eppendorf tubes via cardiac puncture under deep anesthesia and was allowed to clot at room temperature prior to centrifugation and serum collection. Determination of the level of CK was conducted according to the manufacturer's instructions using a standard spectrophotometric method. The data were expressed as units per liter.

Functional Tests

Grip strength of the forearms was assessed using a grip strength meter (GPM-100; MelQuest, Toyama, Japan) according to the manufacturer's instructions. Three forelimb strength measurements were recorded in the morning by an investigator blinded to the treatment conditions. The average grip strength measured each day was used for the subsequent analysis.

Tissue Preparation

The gastrocnemius and tibialis anterior muscles were collected individually using standard dissection methods and cleaned of excess fat, connective tissue, and tendons. Several muscles were frozen in isopentane that was cooled by liquid nitrogen for histological and immunohistochemical analyses, whereas the other muscles were frozen directly in liquid nitrogen for protein extraction and stored at −80°C.

Immunoblotting

Skeletal muscle protein was extracted from the mouse hindlimb muscle samples for immunoblot analysis, as described previously.[67]

Total Collagen Quantification

Frozen gastrocnemius muscles (30-mg portions) were transferred into a Sarstedt tube, and following addition of 600 μL of 6 M HCl, they were hydrolyzed by overnight incubation at 95°C in a heat block. Upon hydrolysis, without any pretreatment, 35 μL of it was used for collagen quantification using a QuickZyme total collagen assay system (QuickZyme Biosciences, Leiden, the Netherlands), and 15 μL was used for the QuickZyme protein assay (QuickZyme Biosciences, Leiden, the Netherlands), which has specifically been developed for protein analysis in acid hydrolysates. The protein data were used for normalization of the unknown quantity of tissue used for hydrolysis.

H&E Staining

Several cryosections of 10 μm were cut in the middle of the muscle belly to obtain the largest myofiber diameter and were then placed on poly-L-lysine-coated slides, air-dried, and stained with H&E. The sections were viewed and photographed using an Olympus digital camera system (Olympus, Tokyo, Japan).

Histological Analysis of Internal Nuclei

Internal nuclei were counted from approximately 200 fibers in at least three separate regions by an investigator blinded to the treatment conditions.

Histological Analysis of Muscle Cross-Sectional Area (CSA)

The muscle CSA was determined using Keyence software (Keyence, Osaka, Japan) to manually trace the circumference of individual fibers. CSA analysis of the muscle was calculated from approximately 5,000 fibers per mouse by an investigator blinded to the treatment conditions.

IgG Immunohistochemistry

IgG staining was used for intracellular IgG [IgG (H+L)] to determine muscle damage. After fixation in 4% paraformaldehyde, gastrocnemius muscle sections were stained with an Alexa Fluor 488 goat anti-mouse IgG (1:500, A-11001; Thermo Fisher Scientific, Waltham, MA, USA) solution in 2% BSA for 2 h at room temperature, washed in

PBS, and mounted with coverslips. Images for IgG staining were taken using a Keyence BZ-X710 (Keyence, Osaka, Japan). 3–4 region of interest images were consequently chosen for each muscle section. All images were analyzed using Keyence software (Keyence, Osaka, Japan) by an investigator blinded to the treatment conditions. The IgG-positive and IgG-negative fibers were individually quantified and then calculated as a percentage of total fibers for each group.

Statistical Analysis

The significance of differences was determined using the Wilcoxon test (Figures 2, 3, 4, 5, 6, and 8; Figures S5, S7–S10, and S12–S14) and ANOVA followed by Tukey's multiple comparison test (Figure 7). Data are expressed as mean ± SE. Statistical significance was set at $p < 0.05$.

SUPPLEMENTAL INFORMATION

Supplemental Information can be found online at https://doi.org/10.1016/j.ymthe.2020.02.006.

AUTHOR CONTRIBUTIONS

H.O., N.S., S.K., and M.A. conceived the project and designed the overall experimental plan. H.O., S.K., and A.Y. performed the proteomics analysis. H.O., N.A., and K.M. performed the laser injury experiments. R.I., T.T., T.A., S.M., and H.W. performed the molecular experiments. Y.K., S.O., K.I., T.S., and R.N. performed the animal experiments. H.O., G.K., and Y.K.H. performed the zebrafish experiments. H.O., N.S., S.K., K.M., and M.A. drafted the manuscript.

ACKNOWLEDGMENTS

We thank Naoko Shimakura, Akiko Machii, Hinako Shigihara, and Maya Narisawa (Tohoku University, Japan) and Katsuhisa Kawai and Kazuhiro Yokoi (Kagawa University, Japan) for general technical support and Tetsuko Sueta and Tomomi Kibushi (Tohoku University, Japan) for animal handling. We also thank Drs. Maki Tateyama and Takafumi Hasegawa (Tohoku University, Japan) for useful technical advice and discussions. We are also grateful to the Jain Foundation for providing us with immortalized human myoblasts and BLA/J mice. This research was partially supported by Intramural Research Grants 26-8 and 29-4 for Neurological and Psychiatric Disorders provided to Y.K.H. and M.A. from the National Center of Neurology and Psychiatry of Japan; the Practical Research Project for Rare/Diseases (15ek0109067h0002 and 18dk0310086) provided to M.A. from the Japan Agency for Medical Research and Development (AMED); Grants-in-Aid for Research on Rare and Intractable Diseases (H26-nanchitou(nan)-ippan-079 and H29-nanchitou(nan)-ippan-030) provided to Y.K.H. and M.A. from the Ministry of Health, Labor and Welfare of Japan; a Grant-in-Aid for Challenging Exploratory Research (26670436) and Scientific Research B (16H05318) provided to M.A., Scientific Research C (18K10822) provided to K.M., Young Scientists A (15H05667) provided to N.S., Young Scientists (18K15437) provided to H.O., and Challenging Exploratory Research (15K14341) provided to G.K. from the Japanese Ministry of Education, Culture, Sports, Science and Technology; the Science Research Promotion Fund in 2014 provided to Y.K.H. from the Promotion and Mutual Aid Corporation for Private Schools of Japan; MEXT-Supported Program for the Strategic Research Foundation at Private Universities (5020-03) provided to Y.K.H.; and by a grant provided to K.M. from the International University of Health and Welfare (IUHW) and the Patients Association for Dysferlinopathy Japan. This research was also supported by the Cooperative Research Project Program of the Joint Usage/Research Center at the Institute of Development, Aging and Cancer, Tohoku University.

REFERENCES

1. Liu, J., Aoki, M., Illa, I., Wu, C., Fardeau, M., Angelini, C., Serrano, C., Urtizberea, J.A., Hentati, F., Hamida, M.B., et al. (1998). Dysferlin, a novel skeletal muscle gene, is mutated in Miyoshi myopathy and limb girdle muscular dystrophy. Nat. Genet. *20*, 31–36.

2. Takahashi, T., Aoki, M., Tateyama, M., Kondo, E., Mizuno, T., Onodera, Y., Takano, R., Kawai, H., Kamakura, K., Mochizuki, H., et al. (2003). Dysferlin mutations in Japanese Miyoshi myopathy: relationship to phenotype. Neurology *60*, 1799–1804.

3. Bashir, R., Britton, S., Strachan, T., Keers, S., Vafiadaki, E., Lako, M., Richard, I., Marchand, S., Bourg, N., Argov, Z., et al. (1998). A gene related to *Caenorhabditis elegans* spermatogenesis factor *fer-1* is mutated in limb-girdle muscular dystrophy type 2B. Nat. Genet. *20*, 37–42.

4. Takahashi, T., Aoki, M., Suzuki, N., Tateyama, M., Yaginuma, C., Sato, H., Hayasaka, M., Sugawara, H., Ito, M., Abe-Kondo, E., et al. (2013). Clinical features and a mutation with late onset of limb girdle muscular dystrophy 2B. J. Neurol. Neurosurg. Psychiatry *84*, 433–440.

5. Illa, I., Serrano-Munuera, C., Gallardo, E., Lasa, A., Rojas-García, R., Palmer, J., Gallano, P., Baiget, M., Matsuda, C., and Brown, R.H. (2001). Distal anterior compartment myopathy: a dysferlin mutation causing a new muscular dystrophy phenotype. Ann. Neurol. *49*, 130–134.

6. Therrien, C., Dodig, D., Karpati, G., and Sinnreich, M. (2006). Mutation impact on dysferlin inferred from database analysis and computer-based structural predictions. J. Neurol. Sci. *250*, 71–78.

7. Doherty, K.R., and McNally, E.M. (2003). Repairing the tears: dysferlin in muscle membrane repair. Trends Mol. Med. *9*, 327–330.

8. Bansal, D., Miyake, K., Vogel, S.S., Groh, S., Chen, C.C., Williamson, R., McNeil, P.L., and Campbell, K.P. (2003). Defective membrane repair in dysferlin-deficient muscular dystrophy. Nature *423*, 168–172.

9. Jaiswal, J.K., Marlow, G., Summerill, G., Mahjneh, I., Mueller, S., Hill, M., Miyake, K., Haase, H., Anderson, L.V., Richard, I., et al. (2007). Patients with a non-dysferlin Miyoshi myopathy have a novel membrane repair defect. Traffic *8*, 77–88.

10. Kokubu, Y., Nagino, T., Sasa, K., Oikawa, T., Miyake, K., Kume, A., Fukuda, M., Fuse, H., Tozawa, R., and Sakurai, H. (2019). Phenotypic drug screening for dysferlinopathy using patient-derived induced pluripotent stem cells. Stem Cells Transl. Med. *8*, 1017–1029.

11. Tanaka, A., Woltjen, K., Miyake, K., Hotta, A., Ikeya, M., Yamamoto, T., Nishino, T., Shoji, E., Sehara-Fujisawa, A., Manabe, Y., et al. (2013). Efficient and reproducible myogenic differentiation from human iPS cells: prospects for modeling Miyoshi myopathy in vitro. PLoS ONE *8*, e61540.

12. Huang, Y., Laval, S.H., van Remoortere, A., Baudier, J., Benaud, C., Anderson, L.V., Straub, V., Deelder, A., Frants, R.R., den Dunnen, J.T., et al. (2007). AHNAK, a novel component of the dysferlin protein complex, redistributes to the cytoplasm with dysferlin during skeletal muscle regeneration. FASEB J. *21*, 732–742.

13. Flix, B., de la Torre, C., Castillo, J., Casal, C., Illa, I., and Gallardo, E. (2013). Dysferlin interacts with calsequestrin-1, myomesin-2 and dynein in human skeletal muscle. Int. J. Biochem. Cell Biol. *45*, 1927–1938.

14. Matsuda, C., Hayashi, Y.K., Ogawa, M., Aoki, M., Murayama, K., Nishino, I., Nonaka, I., Arahata, K., and Brown, R.H., Jr. (2001). The sarcolemmal proteins dysferlin and caveolin-3 interact in skeletal muscle. Hum. Mol. Genet. *10*, 1761–1766.

15. de Morrée, A., Hensbergen, P.J., van Haagen, H.H., Dragan, I., Deelder, A.M., 't Hoen, P.A., Frants, R.R., and van der Maarel, S.M. (2010). Proteomic analysis of the

dysferlin protein complex unveils its importance for sarcolemmal maintenance and integrity. PLoS ONE *5*, e13854.

16. Cai, C., Weisleder, N., Ko, J.K., Komazaki, S., Sunada, Y., Nishi, M., Takeshima, H., and Ma, J. (2009). Membrane repair defects in muscular dystrophy are linked to altered interaction between MG53, caveolin-3, and dysferlin. J. Biol. Chem. *284*, 15894–15902.
17. Lennon, N.J., Kho, A., Bacskai, B.J., Perlmutter, S.L., Hyman, B.T., and Brown, R.H., Jr. (2003). Dysferlin interacts with annexins A1 and A2 and mediates sarcolemmal wound-healing. J. Biol. Chem. *278*, 50466–50473.
18. Ewart, M.A., and Kennedy, S. (2011). AMPK and vasculoprotection. Pharmacol. Ther. *131*, 242–253.
19. Kemp, B.E. (2004). Bateman domains and adenosine derivatives form a binding contract. J. Clin. Invest. *113*, 182–184.
20. Matsuda, C., Miyake, K., Kameyama, K., Keduka, E., Takeshima, H., Imamura, T., Araki, N., Nishino, I., and Hayashi, Y. (2012). The C2A domain in dysferlin is important for association with MG53 (TRIM72). PLoS Curr. *4*, e5035add5038caff5034.
21. Lostal, W., Bartoli, M., Bourg, N., Roudaut, C., Bentaïb, A., Miyake, K., Guerchet, N., Fougerousse, F., McNeil, P., and Richard, I. (2010). Efficient recovery of dysferlin deficiency by dual adeno-associated vector-mediated gene transfer. Hum. Mol. Genet. *19*, 1897–1907.
22. Wang, B., Yang, Z., Brisson, B.K., Feng, H., Zhang, Z., Welch, E.M., Peltz, S.W., Barton, E.R., Brown, R.H., Jr., and Sweeney, H.L. (2010). Membrane blebbing as an assessment of functional rescue of dysferlin-deficient human myotubes via nonsense suppression. J. Appl. Physiol. *109*, 901–905.
23. Jimenez, A.J., Maiuri, P., Lafaurie-Janvore, J., Divoux, S., Piel, M., and Perez, F. (2014). ESCRT machinery is required for plasma membrane repair. Science *343*, 1247136.
24. Defour, A., Van der Meulen, J.H., Bhat, R., Bigot, A., Bashir, R., Nagaraju, K., and Jaiswal, J.K. (2014). Dysferlin regulates cell membrane repair by facilitating injury-triggered acid sphingomyelinase secretion. Cell Death Dis. *5*, e1306.
25. Steinhardt, R.A., Bi, G., and Alderton, J.M. (1994). Cell membrane resealing by a vesicular mechanism similar to neurotransmitter release. Science *263*, 390–393.
26. Lek, A., Evesson, F.J., Lemckert, F.A., Redpath, G.M., Lueders, A.K., Turnbull, L., Whitchurch, C.B., North, K.N., and Cooper, S.T. (2013). Calpains, cleaved mini-dysferlinC72, and L-type channels underpin calcium-dependent muscle membrane repair. J. Neurosci. *33*, 5085–5094.
27. Philippi, S., Bigot, A., Marg, A., Mouly, V., Spuler, S., and Zacharias, U. (2012). Dysferlin-deficient immortalized human myoblasts and myotubes as a useful tool to study dysferlinopathy. PLoS Curr. *4*, RRN1298.
28. Konagaya, Y., Terai, K., Hirao, Y., Takakura, K., Imajo, M., Kamioka, Y., Sasaoka, N., Kakizuka, A., Sumiyama, K., Asano, T., and Matsuda, M. (2017). A highly sensitive FRET biosensor for AMPK exhibits heterogeneous AMPK responses among cells and organs. Cell Rep. *21*, 2628–2638.
29. Kawahara, G., Serafini, P.R., Myers, J.A., Alexander, M.S., and Kunkel, L.M. (2011). Characterization of zebrafish dysferlin by morpholino knockdown. Biochem. Biophys. Res. Commun. *413*, 358–363.
30. Memmott, R.M., Mercado, J.R., Maier, C.R., Kawabata, S., Fox, S.D., and Dennis, P.A. (2010). Metformin prevents tobacco carcinogen—induced lung tumorigenesis. Cancer Prev. Res. (Phila.) *3*, 1066–1076.
31. Cho, Y.S., Lee, J.I., Shin, D., Kim, H.T., Jung, H.Y., Lee, T.G., Kang, L.W., Ahn, Y.J., Cho, H.S., and Heo, Y.S. (2010). Molecular mechanism for the regulation of human ACC2 through phosphorylation by AMPK. Biochem. Biophys. Res. Commun. *391*, 187–192.
32. Krause, U., Bertrand, L., and Hue, L. (2002). Control of p70 ribosomal protein S6 kinase and acetyl-CoA carboxylase by AMP-activated protein kinase and protein phosphatases in isolated hepatocytes. Eur. J. Biochem. *269*, 3751–3759.
33. Gushchina, L.V., Bhattacharya, S., McElhanon, K.E., Choi, J.H., Manring, H., Beck, E.X., Alloush, J., and Weisleder, N. (2017). Treatment with recombinant human MG53 protein increases membrane integrity in a mouse model of limb girdle muscular dystrophy 2B. Mol. Ther. *25*, 2360–2371.
34. Hardie, D.G. (2014). AMPK—sensing energy while talking to other signaling pathways. Cell Metab. *20*, 939–952.
35. Bellinger, A.M., Reiken, S., Carlson, C., Mongillo, M., Liu, X., Rothman, L., Matecki, S., Lacampagne, A., and Marks, A.R. (2009). Hypernitrosylated ryanodine receptor calcium release channels are leaky in dystrophic muscle. Nat. Med. *15*, 325–330.
36. Lanner, J.T., Georgiou, D.K., Dagnino-Acosta, A., Ainbinder, A., Cheng, Q., Joshi, A.D., Chen, Z., Yarotskyy, V., Oakes, J.M., Lee, C.S., et al. (2012). AICAR prevents heat-induced sudden death in RyR1 mutant mice independent of AMPK activation. Nat. Med. *18*, 244–251.
37. Salminen, A., Kaarniranta, K., and Kauppinen, A. (2016). Age-related changes in AMPK activation: role for AMPK phosphatases and inhibitory phosphorylation by upstream signaling pathways. Ageing Res. Rev. *28*, 15–26.
38. Wojtaszewski, J.F., Birk, J.B., Frøsig, C., Holten, M., Pilegaard, H., and Dela, F. (2005). 5'AMP activated protein kinase expression in human skeletal muscle: effects of strength training and type 2 diabetes. J. Physiol. *564*, 563–573.
39. Treebak, J.T., Birk, J.B., Hansen, B.F., Olsen, G.S., and Wojtaszewski, J.F. (2009). A-769662 activates AMPK β_1-containing complexes but induces glucose uptake through a PI3-kinase-dependent pathway in mouse skeletal muscle. Am. J. Physiol. Cell Physiol. *297*, C1041–C1052.
40. Kristensen, D.E., Albers, P.H., Prats, C., Baba, O., Birk, J.B., and Wojtaszewski, J.F. (2015). Human muscle fibre type-specific regulation of AMPK and downstream targets by exercise. J. Physiol. *593*, 2053–2069.
41. Jorgensen, S.B., and Rose, A.J. (2008). How is AMPK activity regulated in skeletal muscles during exercise? Front. Biosci. *13*, 5589–5604.
42. Zhang, B.B., Zhou, G., and Li, C. (2009). AMPK: an emerging drug target for diabetes and the metabolic syndrome. Cell Metab. *9*, 407–416.
43. Foretz, M., Hébrard, S., Guihard, S., Leclerc, J., Do Cruzeiro, M., Hamard, G., Niedergang, F., Gaudry, M., and Viollet, B. (2011). The AMPKγ1 subunit plays an essential role in erythrocyte membrane elasticity, and its genetic inactivation induces splenomegaly and anemia. FASEB J. *25*, 337–347.
44. Cai, C., Masumiya, H., Weisleder, N., Matsuda, N., Nishi, M., Hwang, M., Ko, J.K., Lin, P., Thornton, A., Zhao, X., et al. (2009). MG53 nucleates assembly of cell membrane repair machinery. Nat. Cell Biol. *11*, 56–64.
45. Demonbreun, A.R., Quattrocelli, M., Barefield, D.Y., Allen, M.V., Swanson, K.E., and McNally, E.M. (2016). An actin-dependent annexin complex mediates plasma membrane repair in muscle. J. Cell Biol. *213*, 705–718.
46. Davis, D.B., Doherty, K.R., Delmonte, A.J., and McNally, E.M. (2002). Calcium-sensitive phospholipid binding properties of normal and mutant ferlin C2 domains. J. Biol. Chem. *277*, 22883–22888.
47. Kodera, N., Yamamoto, D., Ishikawa, R., and Ando, T. (2010). Video imaging of walking myosin V by high-speed atomic force microscopy. Nature *468*, 72–76.
48. Uchihashi, T., Iino, R., Ando, T., and Noji, H. (2011). High-speed atomic force microscopy reveals rotary catalysis of rotorless F_1-ATPase. Science *333*, 755–758.
49. Lantier, L., Fentz, J., Mounier, R., Leclerc, J., Treebak, J.T., Pehmøller, C., Sanz, N., Sakakibara, I., Saint-Amand, E., Rimbaud, S., et al. (2014). AMPK controls exercise endurance, mitochondrial oxidative capacity, and skeletal muscle integrity. FASEB J. *28*, 3211–3224.
50. Thomas, M.M., Wang, D.C., D'Souza, D.M., Krause, M.P., Layne, A.S., Criswell, D.S., O'Neill, H.M., Connor, M.K., Anderson, J.E., Kemp, B.E., et al. (2014). Muscle-specific AMPK β1β2-null mice display a myopathy due to loss of capillary density in nonpostural muscles. FASEB J. *28*, 2098–2107.
51. Bujak, A.L., Crane, J.D., Lally, J.S., Ford, R.J., Kang, S.J., Rebalka, I.A., Green, A.E., Kemp, B.E., Hawke, T.J., Schertzer, J.D., and Steinberg, G.R. (2015). AMPK activation of muscle autophagy prevents fasting-induced hypoglycemia and myopathy during aging. Cell Metab. *21*, 883–890.
52. Cerletti, M., Jang, Y.C., Finley, L.W., Haigis, M.C., and Wagers, A.J. (2012). Short-term calorie restriction enhances skeletal muscle stem cell function. Cell Stem Cell *10*, 515–519.
53. Jahnke, V.E., Van Der Meulen, J.H., Johnston, H.K., Ghimbovschi, S., Partridge, T., Hoffman, E.P., and Nagaraju, K. (2012). Metabolic remodeling agents show beneficial effects in the dystrophin-deficient *mdx* mouse model. Skelet. Muscle *2*, 16.
54. Ljubicic, V., Miura, P., Burt, M., Boudreault, L., Khogali, S., Lunde, J.A., Renaud, J.M., and Jasmin, B.J. (2011). Chronic AMPK activation evokes the slow, oxidative

myogenic program and triggers beneficial adaptations in *mdx* mouse skeletal muscle. Hum. Mol. Genet. *20*, 3478–3493.

55. Ljubicic, V., and Jasmin, B.J. (2015). Metformin increases peroxisome proliferator-activated receptor γ co-activator-1α and utrophin a expression in dystrophic skeletal muscle. Muscle Nerve *52*, 139–142.

56. Quattrocelli, M., Barefield, D.Y., Warner, J.L., Vo, A.H., Hadhazy, M., Earley, J.U., Demonbreun, A.R., and McNally, E.M. (2017). Intermittent glucocorticoid steroid dosing enhances muscle repair without eliciting muscle atrophy. J. Clin. Invest. *127*, 2418–2432.

57. Quattrocelli, M., Salamone, I.M., Page, P.G., Warner, J.L., Demonbreun, A.R., and McNally, E.M. (2017). Intermittent glucocorticoid dosing improves muscle repair and function in mice with limb-girdle muscular dystrophy. Am. J. Pathol. *187*, 2520–2535.

58. Chang, M.Y., Ma, T.L., Hung, C.C., Tian, Y.C., Chen, Y.C., Yang, C.W., and Cheng, Y.C. (2017). Metformin inhibits cyst formation in a zebrafish model of polycystin-2 deficiency. Sci. Rep. *7*, 7161.

59. Rovira, M., Arrey, G., and Planas, J.V. (2017). Exercise-induced hypertrophic and oxidative signaling pathways and myokine expression in fast muscle of adult zebrafish. Front. Physiol. *8*, 1063.

60. Sajan, M.P., Bandyopadhyay, G., Miura, A., Standaert, M.L., Nimal, S., Longnus, S.L., Van Obberghen, E., Hainault, I., Foufelle, F., Kahn, R., et al. (2010). AICAR and metformin, but not exercise, increase muscle glucose transport through AMPK-, ERK-, and PDK1-dependent activation of atypical PKC. Am. J. Physiol. Endocrinol. Metab. *298*, E179–E192.

61. Kristensen, J.M., Treebak, J.T., Schjerling, P., Goodyear, L., and Wojtaszewski, J.F. (2014). Two weeks of metformin treatment induces AMPK-dependent enhancement of insulin-stimulated glucose uptake in mouse soleus muscle. Am. J. Physiol. Endocrinol. Metab. *306*, E1099–E1109.

62. Maarbjerg, S.J., Jørgensen, S.B., Rose, A.J., Jeppesen, J., Jensen, T.E., Treebak, J.T., Birk, J.B., Schjerling, P., Wojtaszewski, J.F., and Richter, E.A. (2009). Genetic impairment of AMPKα2 signaling does not reduce muscle glucose uptake during treadmill exercise in mice. Am. J. Physiol. Endocrinol. Metab. *297*, E924–E934.

63. Hardie, D.G. (2014). AMP-activated protein kinase: maintaining energy homeostasis at the cellular and whole-body levels. Annu. Rev. Nutr. *34*, 31–55.

64. Kimmel, C.B., Ballard, W.W., Kimmel, S.R., Ullmann, B., and Schilling, T.F. (1995). Stages of embryonic development of the zebrafish. Dev. Dyn. *203*, 253–310.

65. Kawahara, G., Karpf, J.A., Myers, J.A., Alexander, M.S., Guyon, J.R., and Kunkel, L.M. (2011). Drug screening in a zebrafish model of Duchenne muscular dystrophy. Proc. Natl. Acad. Sci. USA *108*, 5331–5336.

66. Suzuki, N., Aoki, M., Hinuma, Y., Takahashi, T., Onodera, Y., Ishigaki, A., Kato, M., Warita, H., Tateyama, M., and Itoyama, Y. (2005). Expression profiling with progression of dystrophic change in dysferlin-deficient mice (SJL). Neurosci. Res. *52*, 47–60.

67. Suzuki, N., Motohashi, N., Uezumi, A., Fukada, S., Yoshimura, T., Itoyama, Y., Aoki, M., Miyagoe-Suzuki, Y., and Takeda, S. (2007). NO production results in suspension-induced muscle atrophy through dislocation of neuronal NOS. J. Clin. Invest. *117*, 2468–2476.